Supplementary Online Content

Moser DA, Doucet GE, Lee WH, et al. Multivariate associations among behavioral, clinical, and multimodal imaging phenotypes in patients with psychosis. *JAMA Psychiatry*. Published online March 7, 2018. doi:10.1001/jamapsychiatry.2017.4741

This supplementary material has been provided by the authors to give readers additional information about their work.

1. eMethods. Supplemental Methods

1. Participants

One hundred ninety participants were recruited at the Icahn School of Medicine at Mount Sinai (ISMMS), New York. The sample comprised 100 individuals with schizophrenia (SCZ), 40 with psychotic bipolar disorder (BD), and 50 healthy volunteers (Table 1 in main text). The diagnostic status of all participants was based on diagnostic criteria outlined in 5th edition of the Diagnostic and Statistical Manual of Mental Disorders (DSM-5)[1] following personal interview with the Structured Clinical Interview for DSM-5[2] supplemented by information from medical records in the case of patients. Patients were recruited via clinician referrals from the psychiatric services of the Mount Sinai Health System and healthy volunteers were recruited by advertisement in the local press. The eligibility criteria for all participants were (a) 18-45 years; (b) able to communicate fluently in English; (c) IQ>70; (d) no history of head trauma or loss of consciousness; (e) no current or lifetime history of medical or neurological disorders; (f) no lifetime history of DSM-5 substance use disorder; (g) no MRI contra-indications (e.g. metal implants, claustrophobia). Patients were required to fulfil diagnostic DSM-5 criteria for SCZ or BD type-1 while healthy volunteers were included if they had no lifetime personal history of mental disorders and no family history (up to second-degree relatives) of SCZ or BD. The study was approved by the Institutional Review Board of the ISMMS; all participants provided written informed consent prior to study enrollment.

2. Definition of Non-imaging and Imaging Measures

Detailed definitions of the non-imaging and imaging variables are shown in eTable 1 and eTable 2.

3. Multimodal Neuroimaging

We acquired high-resolution structural, diffusion weighted imaging (DWI), resting-state and task-related functional MRI (fMRI) data from all participants as detailed below.

3.1 Imaging Acquisition

Imaging data were acquired at ISMMS on a 3T Skyra scanner (Siemens, Erlangen, Germany) with a 32 channel receiver coil. Anatomical, DWI, resting-state and task acquisitions were identical for all participants. The diffusion data acquisition was acquired using a single-shot spin-echo EPI sequence with a multi-band factor of 3 and monopolar gradient pulse (TR = 3650 ms; TE = 85 ms; FOV = 208×176 mm; matrix = 116×98; 1.8 mm isotropic voxels; FA = 80º; 75 slices). The diffusion sensitizing gradients with a b-value of 1200 s/mm^2 were applied in 64 non-collinear directions (left-to-right phase encoding) with 5 non-diffusion weighted (b0) images. This scan was repeated with phase encoding gradients of reverse polarity to correct for b0- and eddy current-induced distortions and to improve signal-to-noise (SNR) ratio. The resting-state (eyes open) and task-fMRI data were acquired using a T2* single shot echo planar gradient echo imaging sequence with the following parameters: time to echo/repetition time (TE/TR)=35/1000 millisecond (ms), 2.1 mm isotropic resolution, no gap, 70 axial slices for whole brain coverage, field of view (FOV): 206×181×147 mm^3, matrix size: 96×84, 60 degrees flip-angle, multiband (MB) factor 7, blipped CAIPIRINHA (Controlled Aliasing in Parallel Imaging Results in Higher Acceleration) phase-encoding shift = FOV/3, ~2 kHz/Pixel bandwidth with ramp sampling, echo spacing: 0.68 ms, and echo train length 57.1 ms. The duration of the resting-state acquisition was 6 minutes 50 seconds and the duration of the working memory (WM) and emotion recognition (ER) tasks was 11 minutes 37 seconds and 4 minutes and 36 seconds, respectively. Structural images were acquired using a T1-weighted, 3D magnetization-prepared rapid gradient-echo (MPRAGE) sequence (FOV: 256×256×179 mm3, matrix size: 320×320, 0.8 mm isotropic resolution, TE/TR= 2.07/2400 ms, inversion time (TI)=1000 ms, 8 degrees flip-angle with binomial (1, -1) fat saturation, bandwidth 240 Hz/Pixel, echo spacing 7.6 ms, in-plane acceleration (GeneRalized Autocalibrating Partial Parallel Acquisition) factor 2 and total acquisition time of 7 min.

3.2 Processing of Structural Data

Cortical reconstruction and volumetric segmentation of structural datasets was conducted using FreeSurfer image analysis suite (version 5.3.0) which is documented and freely available (http://surfer.nmr.mgh.harvard.edu/). Processing included removal of non-brain tissue using a hybrid watershed/surface deformation procedure[3], automated Talairach transformation, segmentation of the subcortical white matter and deep gray matter volumetric structures[4,5], intensity normalization[6], tessellation of the gray/white matter boundary, automated topology correction[7,8], and surface deformation following intensity gradients to optimally place the gray/white and gray/cerebrospinal fluid borders at the location where the greatest shift in intensity defines the transition to the other

tissue class. This method uses both intensity and continuity information from the entire three dimensional MR volume during segmentation and deformation to produce representations of cortical thickness, calculated as the closest distance from the gray/white boundary to the gray/CSF boundary at each vertex on the tessellated surface[9]. The results were quality controlled using protocols developed by the ENIGMA consortium (http://enigma.ini.usc.edu/). The segmentation yielded 64 cortical thickness measures and 18 subcortical volumetric measures of regions (hippocampus, amygdala, caudate, putamen, nucleus accumbens, pallidum, thalamus, cerebellum and lateral ventricles) (eTable 2). Prior to being entered in further analyses, subcortical volumes were ajusted for variation in intracranial volume (ICV) in accordance to Pintzka et al. (2015)[10] using the following equation: $Vol_{adj} = Vol - \beta * (ICV - \overline{ICV})$, where Vol_{adj} is the ICV-adjusted volume, Vol is the original uncorrected volume, β is the slope from the linear regression of Vol on ICV, ICV is the ICV for the subject and $\overline{ICV}$ is the mean ICV across all subjects. Adjustment using whole brain gray matter volume (WB-GM) instead of ICV was conducted by replacing ICV with total gray matter volume in the above formula. Analyses using either ICV- and WB-GM adjusted measures yielded identical results and we chose to present those following ICV adjustment.

3.3 Processing of DWI Data and Extraction of Tract-Based Fractional Anisotropy

For each subject, diffusion data preprocessing, including brain extraction, susceptibility-induced distortion correction, eddy current correction, and tensor fitting, was performed using standard tools from FSL[11]. The fractional anisotropy (FA) data were then processed using tract-based spatial statistics (TBSS)[12]. Individual FA maps were nonlinearly registered to standard Montreal Neurological Institute (MNI) space. The average FA map was generated and fed into the TBSS skeletonisation algorithm and thresholded at FA > 0.2, resulting in a sample-specific skeleton template. FA voxels were then projected onto the skeleton template to create a FA skeleton in the same space for each individual. The average FA within this white matter skeleton was computed to obtain a global FA for each subject[12]. Regional FA values were extracted from the TBSS skeleton based on the John Hopkins University (JHU) white matter atlas[13]. A total of 38 regional white matter FA values were defined within this atlas[14] by averaging the FA values of the voxels encapsulated in each region (eTable 2).

3.4 Processing of Task and Resting-State fMRI Data

Task and resting-state fMRI data were processed using the Statistical Parametric Mapping software, version 12 (SPM12: http://www.fil.ion.ucl.ac.uk/spm/software/spm12) and the Data Processing and Analysis for Brain Imaging (DPABI) Toolbox[15]. Each fMRI dataset was motion corrected to the first volume with rigid-body alignment; coregistration between the functional scans and the anatomical T1 scan; spatial normalization of the functional images into MNI stereotaxic standard space; spatial smoothing within functional mask with a 6-mm at full-width at half-maximum Gaussian kernel. Resting-state data were additionally preprocessed to correct for head motion using the following steps: wavelet despiking (removing signal transients related to small amplitude (<1 mm) head movements)[16]; detrending; and multiple regression of motion parameters and their derivatives (24-parameter model)[17], as well as white matter, cerebro-spinal fluid (CSF) time series and their linear trends. The white matter and CSF signals were computed using a component-based noise reduction method (CompCor, 5 principal components).[18] Lastly, a bandpass filtering was applied ([0.01-0.1] Hz). Individual resting-state data were excluded if they included severe volume-to-volume head motion above 3 mm or 1 degree.

3.5 fMRI Paradigms: Working Memory and Emotion Recognition

We used the fMRI tasks for WM and ER employed by the Human Connectome Project (HCP; humanconnectomeproject.org).

Working Memory Task: The WM task was presented in a block design. It comprised a sensorimotor control condition (0-back) and a working memory condition (2-back). In the 0-back condition, participants were asked to respond by button press when viewing a predesignated stimulus. In the 2-back condition, participants were instructed to respond by button press when the stimulus they currently viewed matched the one presented 2 trials back. At the start of a block, a written cue (lasting 2.5 seconds) informed participants about the type of condition to follow (0-back or 2-back) and the designated target stimulus for the sensorimotor control condition. Four different stimulus types (faces, places, tools and body parts) were presented in separate blocks. Each stimulus was presented for 7 seconds, followed by a 500 ms inter-stimulus interval. Each run contained 8 blocks of 10 trials, and 4 fixation blocks each lasting 15 seconds. The single-participant images were analyzed via multiple regressions using the linear convolution model, with vectors of onset representing each condition (0- or 2-back). Head motion parameters (i.e., 6 rigid body parameters) were included as regressors of no interest at the first level. Brain regions activated by the WM-task were identified using a random-effects one-sample t-test of the single-participant contrast images for

the 2-back vs 0-back condition (eFigure 1A). The threshold for statistical significance was set to p<0.05 with family-wise error (FWE) correction at voxel level.

Emotion Recognition Task: The ER task was presented as a block design and comprised a control condition (matching shapes) and an emotion condition (matching faces with either an angry or fearful expression). In each condition, participants were asked to indicate by button press which of two shapes (control condition) or which of two faces (emotion condition) presented at the bottom of the screen matched the shape or face at the top of the screen. The task involved 3 control and 3 active blocks each comprising 6 trials of the same condition. Each block was preceded by a 3 second cue indicating whether the trials to follow involved either faces or shapes. Each stimulus was presented for 7 seconds with a 1 second inter-stimulus interval. Brain regions activated by the ER-task were identified using a random-effects one-sample t-test of the single-participant contrast images for the emotional faces vs shape condition. The single-participant images were analyzed via multiple regressions using the linear convolution model, with vectors of onset representing each condition (emotional faces or shapes). Head motion parameters (i.e., 6 rigid body parameters) were included as regressors of no interest at the first level. The threshold for statistical significance was set to p<0.05 with family-wise error (FWE) correction at voxel level.

Alternative Task Analyses: To ascertain that results were not biased by diagnostic group, we also computed a conjunction analysis separately for the WM and ER and extracted beta values of the resulting activation peaks. We repeated the sparse canonical correlation analyses (sCCAs) using these values. The results were identical to our original analyses.

Comparison to the HCP data: To confirm the reliability and generalizability of our findings we conducted the same analyses for the WM and ER tasks using data from the HCP sample (n=823). The analyses of the study and HCP samples yielded overlapping results (eFigure 5).

3.6 Resting-State Networks and Connectivity

In each individual resting-state fMRI dataset we defined the six major resting-state networks (eFigure 6), namely the default-mode network (DMN), central executive network (CEN), salience network (SAL), sensorimotor network (SMN), visual network (VIS), and the auditory (AUD) network using validated masks (available on http://findlab.stanford.edu/functional_ROIs.html). We then calculated within- and between- network functional connectivity (for each individual and each network). Within-network connectivity is defined as the mean strength of the functional connectivity between the regions of a network and reflects functional cohesiveness; while between-network connectivity is defined as the mean strength of the functional connectivity between two distinct networks and reflects functional segregation. For the within-network functional connectivity, we computed the average Pearson's correlation between the time-series of all the voxels of a specific network. For the between-network functional connectivity, we first calculated an average time-series within each network (averaging all the time-series of the voxels part of the network) and then computed the Pearson's correlation between each pair of networks' time-series. These computations resulted into 21 connectivity measures per subject that were further Fisher Z-transformed. No correlation was found between any of these measures and head motion even at p<0.05, uncorrected.

3.7 Quality Assurance and Effect of Head Motion

Two healthy volunteers, 3 patients with BD and 8 patients with SCZ were excluded because of poor data quality in at least one of their scans. After removal of these datasets, comparison between groups (patients, healthy volunteers) on multiple head motion parameters (i.e., mean and maximum scan-to-scan head motion) did not yield significant difference (all: p>0.05).

The framewise displacement was computed using a matlab function freely available (https://github.com/spunt/bspm/blob/master/thirdparty/bramila/bramila_framewiseDisplacement.m) which follows the formula provided by Power et al.[19,20]:

$FD_i = |\Delta d_{ix}| + |\Delta d_{iy}| + |\Delta d_{iz}| + |\Delta \alpha_i| + |\Delta \beta_i| + |\Delta \gamma_i|$,

where i is a volume at time i, $\Delta d_{ix} = d_{(i-1)x} - d_{ix}$ and similarly for the other rigid body parameters [d_{ix} d_{iy} d_{iz} α_i β_i γ_i]. Rotational displacements were converted from degrees to millimeters by calculating displacement on the surface of a sphere of radius 50 mm.

The mean (SD) of the framewise displacement (FD) across fMRI datasets was low across groups [HV: 0.21 (0.08); BD: 0.24 (0.09); SCZ: 0.26 (0.13)]. We tested the effect of head motion based on FD (as defined in eTable 2) by performing all sCCAs with and without including this variable. The mean (SD) of the variate-variable correlations

for FD across modules was -0.22 (0.07). The inclusion of head motion did not influence the overall results (for all modules variable-to-variate correlations resulting from the analyses with head motion included correlated at r>0.96 with those of the original sCCAs).

3.8 Medication: Additional Analyses

We examined the effect of lithium and antidepressants by comparing patients receiving these medications to those that did not on the neuroimaging variables using a series of analyses of covariance with age and sex as covariates; cortical thickness, subcortical volumes, task-related brain activation and intrinsic functional connectivity were examined in separate analyses. None were significant even at $p<0.05$ uncorrected.

4. Examination of Univariate Correlations and Curve Estimation Regression

Prior to data entry, we examined the univariate correlations between imaging and non-imaging variables (eFigure 7) and used curve estimation regression to test each for linearity. We found very few exclusively non-linear relationships and specifically between the emotion recognition task activation in the left visual cortex and moderate activity, between the emotion recognition task activation in the right orbitofrontal cortex and alcohol use and between the thickness of the left transverse temporal gyrus and alcohol use. To ensure that the results of the sCCA were not influenced by these non-linear relationships, we repeated all analyses using the squared values of all the variables. The only canonical correlation value that changed was that for the resting-state connectivity module ($r=0.47$, $p=0.25$) which however remained non-significant. Moreover, the median variable-to-variate correlations resulting from these analyses correlated at $r>0.99$ with those of the original sCCAs.

5. Sparse Canonical Correlation Analyses (sCCA)

5.1 General Principles

Canonical correlation analysis (CCA) is a general method for finding relationships between two multivariate sets of variables (X and Y datasets), all measured in the same individuals. It can be considered as a generalization of multiple linear regression. CCA aims to find those linear combinations (pairs of canonical variates or otherwise modes) of variables in the X dataset and variables in the Y dataset that best express the maximal correlation (i.e., canonical correlation) between the two datasets. Suppose we wished to examine the relationship between the variables in the X dataset (variables x_1, x_2,…., x_p) and the Y dataset (variables y_1, y_2,...., y_q). The correlations between the canonical variates are the canonical correlations. A typical CCA would progress in *n* iterative steps each forming two linear combinations following the generic formula: $W_n = a_{1n}x_1 + a_{2n}x_2 + \ldots + a_{np}x_p$ and $V_n = b_{1n}y_1 + b_{1n}y_2 + \ldots + b_{1nq}y_q$, such that the correlation C_n of W_n and V_n is maximum and the correlations between (W_n, W_{n+1}) and (V_n, V_{n+1}) are zero.

In recent years, sparse CCA (sCCA) has been developed to address the drawbacks of the conventional approach. First, sCCA does not assume that the variables in the datasets are uncorrelated. Second, in conventional CCA, all weights contributing to any significant relation between datasets are non-zero and is therefore not possible to make inferences about individual variables. By contrast, in sCCA some of the elements of the canonical vectors are estimated as exactly zero using penalty functions. The canonical variates then only depend on the subset of the variables with non-zero elements of the estimated canonical vectors. This renders sCCA results easier to interpret when dealing with large datasets. Finally, sCCA allows the investigation of datasets possessed of more features than samples, which is often the case in neuroimaging.

5.2. sCCA in the Current Study

In this study we used a sparse CCA approach which uses an L_1 penalty to impose sparsity. The same sCCA approach was used examine the relationship of non-imaging data with the global multimodal and the modular neuroimaging datasets. Non-imaging and neuroimaging variables were standardized to a mean of 0 and a standard deviation of 1 and entered into sCCAs implemented in MatlabR2015b using an in-house script. For each analysis, we computed the sparse parameters by running the sCCA with a range of candidate values (from $0.1x\sqrt{p}$ to $1x\sqrt{p}$, at 0.1 increments, where p is the number of features in that view of the data) for each imaging and behavioral-health dataset, and then fitted the resulting models. We selected the optimal sparse criteria combination based on the parameters that corresponded to the values of the model that maximized the sCCA correlation value. We then computed the optimal sCCA model and determined its significance using permutations. Accordingly, the imaging dataset was permuted 5,000 times before undergoing the exact same analysis as the original data. This permutation procedure was done using the tool Permutation Analysis of Linear Models (PALM) freely available

(https://fsl.fmrib.ox.ac.uk/fsl/fslwiki/PALM). The p-value was defined as the number of permutations that resulted in a higher correlation than the original data divided by the total number of permutations. Thus the p-value is explicitly corrected for multiple testing as it is compared against the null distribution of maximal correlation values across all estimated sCCAs. For each permutation we tested all sparsity criteria combinations as for the original data and then extracted the sCCA correlation with the highest coefficient among the tested options, independently of whether this combination was the same as in the original data. In this way we ensured that we did not underestimate the chance of a permutation achieving the same or higher value than the original data. The threshold for statistical significance for each analysis was set at $p<0.05$. Only sCCA modes considered both statistically significant and stable (following the reliability analyses described in section 6) were considered. We then computed Pearson's correlations between each variable and the opposing variate (i.e., each non-imaging variable to the neuroimaging variate and vice versa) and assessed their reliability as described below in section 6.

6. Reliability analyses

6.1 Reliability of the Overall sCCA Correlations for each Module

To confirm the reliability of the sCCA results (for each sCCA model examined) we created training datasets by randomly resampling half of the sample 5000 times and repeating the sCCAs on the training sets. We then applied the sCCA weights from each training-set to the other half of the sample (test-sets) to test for over-fitting. In addition, we examined the reliability of the overall sCCA models using the leave-one-out approach.

We examined the stability of each sCCA as a function of sample size and composition. To this purpose, we applied a bootstrap resampling approach by randomly resampling 10% to 150% from the original sample (in 10% increments) 1000 times. This resampling generates subsets of the original dataset that have variable composition in terms of diagnostic groups (healthy volunteers, patients with SCZ, patients with BD). We then conducted sCCAs on each bootstrapped subset.

6.2 Reliability of Variable-to-variate Correlations

We used the redundancy-reliability score (RR-Score) as a measure of the stability of the variable-to-variate correlations for each sCCA model examined. The RR-score was based on the 5000 resampled test-sets that were created as described above in the reliability analysis of the sCCA models. We calculated as:

$$RR^j = \frac{\left|corr\left(r_W^{TS}, r_W^j\right)\right| + \left|corr\left(r_V^{TS}, r_V^j\right)\right|}{2}$$

where W denotes imaging-variable to non-imaging variate. V denotes non-imaging-variable to imaging variate.

r_W^j are the variable-to-variate correlation between imaging variables and the non-imaging variate of test-set j

r_V^j are the variable-to-variate correlation between non-imaging variables and the imaging variate of test-set j

r_W^{TS} are the mean variable-to-variate correlation values between imaging variables and the non-imaging variate of the 5000 test-sets.

r_V^{TS} are the mean variable-to-variate correlation values between non-imaging variables and the imaging variate of the 5000 test-sets.

The RR-score is thus an index of similarity between all test-sets. RR-scores that are close to 1 indicate that a test-set would have yielded very similar results as the mean of test-sets. We report the median RR-score and the standard-deviation in eResults for the first three modes of each sCCA.

2. **eResults.** Supplemental Results

1. Case-Control Analyses

We conducted a number of conventional analyses focusing on diagnostic group comparisons to ensure the complete description of the characteristics of the sample. These analyses are peripheral to the aim and findings of this study. The results are summarized in eFigures 1-4 and eTables 3-4.

2. Selection of sCCA Modes

For each sCCA, we only reported modes that were both significant and reliable based on the reliability analyses. Only the first mode satisfied both conditions in the sCCAs for global, cortical thickness, subcortical volume, task-related brain connectivity and white matter FA as shown in eFigure 5. The RR-score ranges between 0 and 1; a value of 0 indicates no correlation between the canonical correlations generated from the randomly resampled 5000 test-sets created during the reliability analyses and a value of 1 indicates complete agreement. RR-scores indicated that the first mode yielded reliable or very reliable solutions for all significant sCCAs (global: median RR-score was 0.92, SD = 0.03; cortical thickness: median 0.91, SD =0.03; subcortical volumes: median 0.84, SD = 0.11, brain-activation: median = 0.87, SD = 0.11, white matter FA: median = 0.78, SD = 0.14.) but that the second and third modes (and onwards) did not yield reliably reproducible solutions (all median RR-scores < 0.55).

3. Reliability of the Overall sCCA Correlations for each Module

The leave-one-out analyses indicated that the global and the modular sCCAs for cortical thickness, subcortical volumes and task activation were stable (the weights of each leave-one-out analysis correlated above 0.92 with the sCCA weights in the full dataset). When half the sample was randomly resampled 5000 times, global and modular sCCAs yielded similar correlations in all cases; the mean (standard-deviation) were r=0.67 (0.04) for the global sCCA; r=0.68 (0.04) for the cortical thickness sCCA; r=0.57 (0.04) for subcortical volume; r=0.50 (0.05) for task-related activation, and r=0.51 (0.05) for white matter fractional anisotropy. We then applied the weights of each sCCA resample to the remaining half of the sample (using it as a test-set). The mean (standard-deviation) of the scores indicated that the sCCA results held predictive value for the global sCCA [r = 0.53 (0.07)], cortical thickness [r =0.52 (0.07)], subcortical volume [r = 0.30 (0.10)], task activation [r = 0.26 (0.11)], and white matter fractional anisotropy [r=0.19 (0.12)].

4. Effect of Sample Size on the Reproducibility of the sCCA Correlations

As shown in eFigure 9, the results of the significant models (global, cortical thickness, subcortical volume, task-based activation, white matter FA) were stable for any sample larger than approximately 70% of the original (i.e., from n>124). This was not the case for the resting-state connectivity module where the reproducibility of the results dropped as sample size increased indicating that the correlation between the non-imaging and resting-state connectivity variate are mainly influenced by the constitution of the sample.

5. Effect of Diagnostic Group on the sCCA Correlations

eFigure 10.1 depicts the distribution of the participant-specific correlations for each diagnostic group and indicates that all groups behave similarly within the sCCA models. We used Fisher r-to-z transformation[21] to compare pairwise r-values. We found no significant group differences in either the global or the modular analyses (all |z-scores| <2.3, p>0.06, FDR corrected).

eFigure 10.2 depicts the distribution of the participant-specific correlations for the healthy volunteers versus patients, when the patients with bipolar disorder and with schizophrenia were collapsed into on a single group. We found no significant group differences in either the global or the modular analyses (all |z-scores| <2.5, p>0.08, FDR corrected).

In addition, we conducted the global and modular sCCAs for each diagnostic group separately. For the healthy volunteers, variables related to positive and negative psychotic symptoms and psychotic medication were not included in the sCCAs (eFigure 11).

6. Primary and Reliability Analyses for the Variable-to-variate Correlations across sCCAs

We present the correlation (r) of each variable-to-variate pair for the primary analyses. Additionally we present the mean and standard deviation of the correlation value of each variable-to-variate combination among the 5000 test-

sets used in the reliability analyses (r^{TS}). The correlations between each non-imaging variable to the global and modular variates are shown in eTable 7.

The correlations between each imaging variable and the non-imaging variate are shown separately for the global (eTable 8), cortical thickness (eTable 9), subcortical volume (eTable 10), task-related brain activation (eTable 11) and white matter FA (eTable 12). The reliability of these findings for the top-five non-imaging variables is visually depicted in eFigure 12.

4. eDiscussion. Supplemental Discussion

1. Resting State Module

We found that the only sCCA that was not significant concerned the resting-state module. This was surprising since alterations in resting-state network connectivity have been found both in schizophrenia and in bipolar disorder.[22-25] Additionally, previous studies have reported associations between resting-state network connectivity and BMI, cognition and physical health.[26-29] During the reliability analyses we applied a bootstrap resampling approach by randomly resampling 10% to 150% from the original sample (in 10% increments) 1000 times. This approach generated samples with variable composition in terms of diagnostic grouping (healthy volunteers, patients with SCZ, patients with BD) and also variable distributions in terms of the values of the imaging and non-imaging measures. As shown in eFigure 5 the sCCA correlation for the resting-state module declined as sample size increased. We thus consider that the pattern of correlations between resting-state and non-imaging variables is dependent on sample composition and unlikely to generalize across samples. This interpretation requires confirmation in future studies.

2. Effect of Diagnosis on variable-to-variate correlations

As shown in eFigure 7, some variable-to-variate correlations for the non-imaging data showed numerical variability across diagnostic groups while others did not. In general, age and BMI always had negative associations with the neuroimaging variables while the association with IQ was positive. Age showed the least transdiagnostic variability with the exception of white matter FA where its contribution was minimal for the bipolar group. The correlation of BMI with the imaging measures seemed to be higher for healthy individuals and lower for patients, particularly for those diagnosed with schizophrenia. A similar pattern was also observed for IQ but in this case the contribution of IQ was lowest in patients with bipolar disorder. These observations are intriguing and require confirmation in further studies.

3. Practical implications for future neuroimaging analyses

The analytical approach that we used here could be applied to other study samples in order to determine the pattern of covariation between the imaging and non-imaging variables being considered. The weights of the variable-to-variate correlation could be used to inform about the key sources of variance in the sample and guide choices as to how these could be addressed. The specific approach would depend on the questions that each study attempts to address and could range from simple solution involving regressing out the effect of key sources of "unwanted variance" at the level of individual variables prior to case-control comparisons to more sophisticated multivariate models.

eTables. Supplemental Tables

eTable 1. Definitions of the Nonimaging Variables

Variable name	Definition
Age	Age in years on the day of study assessment
Sex	Male or female
Intelligence quotient (IQ)	Full-scale IQ based on Wechsler Abbreviated Scale of Intelligence, 2nd edition[30]
Body mass index (BMI)	Weight (kilograms)/height (meters)^2
Physical activity	Physical activity was assessed using the short form of the International Physical Activity Questionnaire[31] which has shown good test-retest reliability and convergent validity with accelerometers. We considered the number of days in the preceding week when participants were engaged in moderate physical activity (metabolic equivalent of task ≥3)[32] such as brisk walking for at least 10 continuous minutes.
Sedentary time	Sedentary time was assessed using the short form of the International Physical Activity Questionnaire[31]. We considered the time spent sitting or reclining while awake on a single typical day within the preceding 7 days. Participants were categorized into 3 groups (Low: less than 30min; Intermediate: between 30 and 60 min; High: more than 60min).
Lifetime cannabis use	Recreational use only (i.e., not fulfilling DSM-5 diagnostic criteria for substance use disorder) was allowed. Participants were categorized into those endorsing any or no cannabis use.
Lifetime substance use (excluding cannabis)	Recreational use only (i.e., not fulfilling DSM-5 diagnostic criteria for substance use disorder) of cocaine, opioids or amphetamines was allowed. Participants were categorized into those endorsing any or no substance use.
Current Smoking	Participants were categorized into 3 groups (1: Daily; 2: Some days; 3: Not at all).
Current Alcohol use	Recreational use only (i.e., not fulfilling DSM-5 diagnostic criteria for alcohol use disorder) was allowed. Alcohol use was coded on a scale of 1(2 units or less every day) to 9 (never use alcohol).
Family History of Depression	Defined as at least one case of major depressive episode in a relative up to 2nd degree.
Family History of Psychosis	Defined as at least one case of schizophrenia, bipolar disorder or spectrum diagnosis in relative up to 2nd degree.
Experience of trauma	Experience of trauma was assessed using the Brief Trauma Questionnaire[33], a 10-item self-report questionnaire that identifies lifetime exposure to the most common types of traumatic experiences, including war traumas, serious car accidents, natural disasters, exposure to violent death, life-threatening illness, and physical or sexual abuse. Participants were categorized into those that did or did not endorse any traumatic event.
Positive symptoms	Based on the Brief Psychiatric Rating Scale[34] positive symptoms factor score.
Negative symptoms	Based on the Brief Psychiatric Rating Scale[34] negative symptoms factor score.

eTable 1. Definitions of the Nonimaging Variables	
Depression/anxiety	Based on the Brief Psychiatric Rating Scale[34] depression/anxiety factor score.
Mania/disorganization	Based on the Brief Psychiatric Rating Scale[34] mania and disorganization factor score.
Antipsychotic dose	Antipsychotic dose on the day of scanning converted into chlorpromazine equivalents.[35]
Head Motion	
Average Head Motion	Framewise displacement (FD)[19] during fMRI scans. For the resting state functional connectivity module the FD of the resting state scan was used. For the task activation module the FD of both tasks was used. For all other analyses the mean of all three was used.

eTable 2. Definition of the Imaging Variables	
Cortical Thickness	
Caudal anterior cingulate cortex	Derived from cortical reconstruction using Freesurfer v5.3.; left and right measures were considered separately
Caudal middle frontal gyrus	Derived from cortical reconstruction using Freesurfer v5.3.; left and right measures were considered separately
Cuneus	Derived from cortical reconstruction using Freesurfer v5.3.; left and right measures were considered separately
Entorhinal cortex	Derived from cortical reconstruction using Freesurfer v5.3.; left and right measures were considered separately
Fusiform gyrus	Derived from cortical reconstruction using Freesurfer v5.3.; left and right measures were considered separately
Inferior parietal lobule	Derived from cortical reconstruction using Freesurfer v5.3.; left and right measures were considered separately
Inferior temporal gyrus	Derived from cortical reconstruction using Freesurfer v5.3.; left and right measures were considered separately
Lateral occipital gyrus	Derived from cortical reconstruction using Freesurfer v5.3.; left and right measures were considered separately
Lateral orbitofrontal gyrus	Derived from cortical reconstruction using Freesurfer v5.3.; left and right measures were considered separately
Lingual gyrus	Derived from cortical reconstruction using Freesurfer v5.3.; left and right measures were considered separately
Medial orbitofrontal gyrus	Derived from cortical reconstruction using Freesurfer v5.3.; left and right measures were considered separately
Middle temporal gyrus	Derived from cortical reconstruction using Freesurfer v5.3.; left and right measures were considered separately
Parahippocampal gyrus	Derived from cortical reconstruction using Freesurfer v5.3.; left and right measures were considered separately
Paracentral gyrus	Derived from cortical reconstruction using Freesurfer v5.3.; left and right measures were considered separately
Pars opercularis	Derived from cortical reconstruction using Freesurfer v5.3.; left and right measures were considered separately
Pars orbitalis	Derived from cortical reconstruction using Freesurfer v5.3.; left and right measures were considered separately
Pars triangularis	Derived from cortical reconstruction using Freesurfer v5.3.; left and right measures were considered separately

eTable 2. Definition of the Imaging Variables	
Pericalcarine gyrus	Derived from cortical reconstruction using Freesurfer v5.3.; left and right measures were considered separately
Postcentral gyrus	Derived from cortical reconstruction using Freesurfer v5.3.; left and right measures were considered separately
Posterior cingulate cortex	Derived from cortical reconstruction using Freesurfer v5.3.; left and right measures were considered separately
Precentral gyrus	Derived from cortical reconstruction using Freesurfer v5.3.; left and right measures were considered separately
Precuneus	Derived from cortical reconstruction using Freesurfer v5.3.; left and right measures were considered separately
Rostral anterior cingulate cortex	Derived from cortical reconstruction using Freesurfer v5.3.; left and right measures were considered separately
Rostral middle frontal gyrus	Derived from cortical reconstruction using Freesurfer v5.3.; left and right measures were considered separately
Superior frontal gyrus	Derived from cortical reconstruction using Freesurfer v5.3.; left and right measures were considered separately
Superior parietal lobule	Derived from cortical reconstruction using Freesurfer v5.3.; left and right measures were considered separately
Superior temporal gyrus	Derived from cortical reconstruction using Freesurfer v5.3.; left and right measures were considered separately
Supramarginal gyrus	Derived from cortical reconstruction using Freesurfer v5.3.; left and right measures were considered separately
Frontal pole	Derived from cortical reconstruction using Freesurfer v5.3.; left and right measures were considered separately
Temporal pole	Derived from cortical reconstruction using Freesurfer v5.3.; left and right measures were considered separately
Transverse temporal gyrus	Derived from cortical reconstruction using Freesurfer v5.3.; left and right measures were considered separately
Insula	Derived from cortical reconstruction using Freesurfer v5.3.; left and right measures were considered separately
Subcortical Volumes	
Thalamus	Derived from segmentation using Freesurfer v5.3.; left and right measures were considered separately following ICV correction
Hippocampus	Derived from segmentation using Freesurfer v5.3.; left and right measures were considered separately

eTable 2. Definition of the Imaging Variables	
	following ICV correction
Caudate nucleus	Derived from segmentation using Freesurfer v5.3.; left and right measures were considered separately following ICV correction
Nucleus Accumbens	Derived from segmentation using Freesurfer v5.3.; left and right measures were considered separately following ICV correction
Pallidum	Derived from segmentation using Freesurfer v5.3.; left and right measures were considered separately following ICV correction
Putamen	Derived from segmentation using Freesurfer v5.3.; left and right measures were considered separately following ICV correction
Amygdala	Derived from segmentation using Freesurfer v5.3.; left and right measures were considered separately following ICV correction
Cerebellum	Derived from segmentation using Freesurfer v5.3.; left and right measures were considered separately following ICV correction
Lateral ventricles	Derived from segmentation using Freesurfer v5.3.; left and right measures were considered separately following ICV correction
Diffusion Weighted Imaging Fractional Anisotropy	
Genu of corpus callosum	Mean regional fractional anisotropy
Body of corpus callosum	Mean regional fractional anisotropy
Splenium of corpus callosum	Mean regional fractional anisotropy
Fornix	Mean regional fractional anisotropy
Right Anterior limb of internal capsule	Mean regional fractional anisotropy
Left Anterior limb of internal capsule	Mean regional fractional anisotropy
Right Posterior limb of internal capsule	Mean regional fractional anisotropy
Left Posterior limb of internal capsule	Mean regional fractional anisotropy
Right Retrolenticular part of internal capsule	Mean regional fractional anisotropy
Left Retrolenticular part of internal capsule	Mean regional fractional anisotropy
Right Anterior corona radiata	Mean regional fractional anisotropy
Left Anterior corona radiata	Mean regional fractional anisotropy
Right Superior corona radiata	Mean regional fractional anisotropy
Left Superior corona radiata	Mean regional fractional anisotropy
Right Posterior corona radiata	Mean regional fractional anisotropy
Left Posterior corona radiata	Mean regional fractional anisotropy
Right Posterior thalamic radiation	Mean regional fractional anisotropy
Left Posterior thalamic radiation	Mean regional fractional anisotropy
Right External capsule	Mean regional fractional anisotropy
Left External capsule	Mean regional fractional anisotropy
Right Cingulum (cingulate gyrus)	Mean regional fractional anisotropy
Left Cingulum (cingulate gyrus)	Mean regional fractional anisotropy

eTable 2. Definition of the Imaging Variables	
Right Cingulum (hippocampal portion)	Mean regional fractional anisotropy
Left Cingulum (hippocampal portion)	Mean regional fractional anisotropy
Left Fornix (cres) / Stria terminalis	Mean regional fractional anisotropy
Right Fornix (cres) / Stria terminalis	Mean regional fractional anisotropy
Right Superior longitudinal fasciculus	Mean regional fractional anisotropy
Left Superior longitudinal fasciculus	Mean regional fractional anisotropy
Right Superior fronto-occipital fasciculus	Mean regional fractional anisotropy
Left Superior fronto-occipital fasciculus	Mean regional fractional anisotropy
Right Inferior fronto-occipital fasciculus	Mean regional fractional anisotropy
Left Inferior fronto-occipital fasciculus	Mean regional fractional anisotropy
Right Uncinate fasciculus	Mean regional fractional anisotropy
Left Uncinate fasciculus	Mean regional fractional anisotropy
Right Internal capsule	Mean regional fractional anisotropy
Left Internal capsule	Mean regional fractional anisotropy
Right Corona radiata	Mean regional fractional anisotropy
Left Corona radiata	Mean regional fractional anisotropy
Task-related Brain Activation: Working Memory	
Right inferior parietal lobule	Beta-value from corresponding volume of interest
Left inferior parietal lobule	Beta-value from corresponding volume of interest
Right dorsal anterior cingulate cortex	Two peaks. Beta-value from corresponding volume of interest
Left dorsal anterior cingulate cortex	Beta-value from corresponding volume of interest
Right inferior occipital gyrus	Beta-value from corresponding volume of interest
Left inferior occipital gyrus	Beta-value from corresponding volume of interest
Left lingual gyrus	Beta-value from corresponding volume of interest
Right middle frontal gyrus	Beta-value from corresponding volume of interest
Left middle frontal gyrus	Beta-value from corresponding volume of interest
Right middle temporal gyrus	Beta-value from corresponding volume of interest
Left middle temporal gyrus	Beta-value from corresponding volume of interest
Task-related Brain Activation: Emotion Recognition	
Right inferior occipital gyrus	Beta-value from corresponding volume of interest
Left inferior occipital gyrus	Beta-value from corresponding volume of interest
Right fusiform gyrus	Beta-value from corresponding volume of interest
Left fusiform gyrus	Beta-value from corresponding volume of interest
Right amygdala	Beta-value from corresponding volume of interest
Left amygdala	Beta-value from corresponding volume of interest
Right middle frontal gyrus	Beta-value from corresponding volume of interest
Left middle frontal gyrus	Beta-value from corresponding volume of interest
Right inferior frontal gyrus	Beta-value from corresponding volume of interest
Left inferior frontal gyrus	Beta-value from corresponding volume of interest
Right calcarine gyrus	Beta-value from corresponding volume of interest
Left calcarine gyrus	Beta-value from corresponding volume of interest
Right superior temporal gyrus	Beta-value from corresponding volume of interest
Precuneus	Beta-value from corresponding volume of interest
Resting-state Functional Connectivity (within-network)	

eTable 2. Definition of the Imaging Variables	
Default Mode Network (DMN)	Average Pearson's correlation between the time-series of all the voxels of a specific network
Central Executive Network (CEN)	Average Pearson's correlation between the time-series of all the voxels of a specific network
Salience Network (SAL)	Average Pearson's correlation between the time-series of all the voxels of a specific network
Sensorimotor Network (SMN)	Average Pearson's correlation between the time-series of all the voxels of a specific network
Visual Network (VIS)	Average Pearson's correlation between the time-series of all the voxels of a specific network
Auditory network (AUD)	Average Pearson's correlation between the time-series of all the voxels of a specific network
Resting-state Functional Connectivity (between-network)	
DMN-CEN	Pearson's correlation between the networks' time-series
DMN-SAL	Pearson's correlation between the networks' time-series
DMN-SMN	Pearson's correlation between the networks' time-series
DMN-VIS	Pearson's correlation between the networks' time-series
DMN-AUD	Pearson's correlation between the networks' time-series
CEN-SAL	Pearson's correlation between the networks' time-series
CEN-SMN	Pearson's correlation between the networks' time-series
CEN-VIS	Pearson's correlation between the networks' time-series
CEN-AUD	Pearson's correlation between the networks' time-series
SAL-SMN	Pearson's correlation between the networks' time-series
SAL-VIS	Pearson's correlation between the networks' time-series
SAL-AUD	Pearson's correlation between the networks' time-series
SMN-VIS	Pearson's correlation between the networks' time-series
SMN-AUD	Pearson's correlation between the networks' time-series
VIS-AUD	Pearson's correlation between the networks' time-series

eTable 3. Case-Control Differences in Brain Activation in the Working Memory Task (2-back>0-back)

Region	Laterality				Cluster Size	t-value	Comments
		x	y	z			
Inferior Parietal Lobule	Left	-44	-36	40	4767	5.73	HV> all pts; HV >pts with SCZ; HV >pts with BD
Medial Prefrontal Cortex	Left	-6	14	56	4091	5.48	HV > all pts; HV >pts with SCZ; HV >pts with BD
Insula	Left	-40	20	-4	382	5.25	HV > all pts; HV >pts with SCZ
Middle Temporal Gyrus	Right	60	-52	-10	245	4.75	HV > all pts; HV>pts with SCZ
Thalamus	Left	-8	-14	8	657	4.45	HV> all pts
Brainstem	Left	-2	-26	-12	726	5.15	HV> all pts
Cerebellum	Left	-32	-60	-28	959	5.15	HV> all pts; HV>pts with SCZ
Cerebellum	Left	-4	-44	-18	353	4.53	HV> all pts
Cerebellum	Right	6	-72	-42	195	4.91	HV> all pts
Cerebellum	Right	28	-56	-34	353	4.00	HV> all pts; HV>pts with SCZ; HV>pts with BD

Family wise error corrected cluster wide significance of $p < 0.05$ at a cluster forming threshold of uncorrected $p<0.001$; BD=bipolar disorder; HV=healthy volunteers; pts=patients; SCZ=schizophrenia

eTable 4. Case-Control Differences in Brain Activation in the Emotional Recognition Task (Emotional Face Matching > Shape Matching)

Region	Laterality	MNI Coordinates			Cluster Size	t-value	Comments
		x	y	z			
Fusiform Gyrus	Left	-30	-84	-2	329	4.55	HV<all patients

Family wise error corrected cluster wide significance of p <0.05 at a cluster forming threshold of uncorrected p<0.001; HV=healthy volunteers.

eTable 5. Suprathreshold Clusters of Task-Related Activation in the Working Memory Task (2-back > 0-back)

Region	Laterality	Co-ordinates			Cluster Size
		x	y	z	
Inferior Parietal Lobule	Right	44	-38	42	9104
	Left	-42	-48	44	
Middle Frontal Gyrus	Right	28	8	58	27417
	Left	-28	4	60	
Dorsal Anterior Cingulate Cortex	Right	2	22	44	
	Left	-2	24	44	
	Right	4	12	26	198
Inferior Occipital Gyrus	Left	-12	-94	0	513
	Right	16	-90	-8	35
Lingual Gyrus	Left	-28	-86	-16	79
Middle Temporal Gyrus	Left	-50	-38	-6	76
	Right	50	-42	-2	46

Coordinates are reported in MNI Space; x=axial; y=coronal; z=sagittal; p<0.05 familywise error corrected at voxel level, all clusters are at T>5.

eTable 6. Suprathreshold Clusters of Task-Related Activation in the Emotion Recognition Task					
Region	**Laterality**	**Co-ordinates**			**Cluster Size**
		x	**y**	**z**	
Fusiform Gyrus	Right	40	-50	-22	1904
Inferior Occipital Gyrus	Right	32	-96	-2	
	Left	-26	-96	-6	1425
Fusiform Gyrus	Left	-38	-56	-20	
Amygdala /Hippocampus	Right	18	-4	-12	40
	Left	-16	-4	-12	49
Middle Frontal Gyrus	Right	46	12	30	299
	Left	-44	20	24	149
Cuneus	Right	8	-84	2	44
	Left	-6	-84	0	33
Superior Temporal Gyrus	Right	48	-40	12	31
Inferior Frontal Gyrus	Left	-42	28	-14	42
	Right	32	36	-10	30
Precuneus	Bilateral	2	-64	34	30
Coordinates are reported in MNI Space; x=axial; y=coronal; z=sagittal; p<0.05 familywise error corrected at voxel level, all clusters are at T>5.					

eTable 7. Correlations Between the Individual Nonimaging Variables and the Imaging Variates for the Global and Modular Analyses in the Original Data Set (r) and Resampled Test-Sets (r^{TS})

	Global		Cortical thickness		Subcortical volume		Task-based Activation		White Matter Fractional Anisotropy	
Variable	**r-value**	**Mean r^{TS} (SD)**	**r-value**	**Mean r^{TS} (SD)**	**r-value**	**Mean r^{TS} (SD)**	**r-value**	**Mean r^{TS} (SD)**	**r-value**	**Mean r^{TS} (SD)**
Age	-0.53	-0.48 (0.06)	-0.5	-0.46 (0.07)	-0.44	-0.39 (0.10)	-0.28	-0.23 (0.08)	-0.36	-0.24 (0.13)
Sex	0.18	0.16 (0.08)	0.16	0.15 (0.09)	0.37	0.23 (0.10)	0.03	0.01 (0.08)	0.22	0.19 (0.13)
Intelligence quotient	0.36	0.35 (0.06)	0.39	0.35 (0.07)	-0.09	-0.12 (0.09)	0.34	0.29 (0.09)	0.2	0.15 (0.09)
Body mass index	-0.25	-0.22 (0.07)	-0.28	-0.26 (0.07)	-0.15	-0.11 (0.10)	-0.22	-0.17 (0.08)	-0.26	-0.19 (0.11)
Physical activity	0.13	0.13 (0.08)	0.12	0.12 (0.09)	0.05	0.07 (0.09)	-0.05	-0.03 (0.09)	0.06	0.05 (0.08)
Sedentary time	0.15	0.16 (0.07)	0.19	0.18 (0.07)	-0.02	-0.07 (0.09)	0.22	0.21 (0.09)	0.06	0.04 (0.09)
Lifetime cannabis use	0.13	0.11 (0.07)	0.1	0.09 (0.08)	0.23	0.17 (0.09)	-0.03	-0.02 (0.08)	0.09	0.07 (0.08)
Lifetime substance use	0.19	0.17 (0.07)	0.15	0.15 (0.08)	0.33	0.28 (0.09)	-0.01	-0.02 (0.08)	0.06	0.04 (0.08)
Current alcohol use	-0.06	-0.06 (0.07)	-0.11	-0.1 (0.08)	0.14	0.18 (0.10)	-0.1	-0.09 (0.09)	-0.15	-0.11 (0.09)
Current smoking	0.1	0.09 (0.08)	0.13	0.12 (0.09)	-0.08	-0.08 (0.09)	0.1	0.09 (0.08)	0.01	-0.03 (0.09)
Family History of Depression	-0.04	-0.03 (0.08)	-0.03	-0.03 (0.08)	-0.12	-0.10 (0.09)	0	-0.01 (0.09)	-0.02	-0.02 (0.09)
Family History of Psychosis	0.04	0.05 (0.08)	0.11	0.1 (0.08)	-0.02	-0.10 (0.11)	0.1	0.08 (0.08)	0.14	0.09 (0.09)
Experience of trauma	-0.11	-0.11 (0.08)	-0.13	-0.13 (0.08)	0.01	0.00 (0.08)	-0.06	-0.06 (0.08)	0.04	0.02 (0.09)
Positive symptoms	-0.13	-0.15 (0.08)	-0.22	-0.2 (0.08)	0.11	0.15 (0.10)	-0.17	-0.15 (0.08)	-0.05	-0.06 (0.09)
Negative symptoms	-0.02	-0.04 (0.08)	-0.08	-0.08 (0.08)	0.23	0.22 (0.10)	-0.1	-0.09 (0.08)	0.09	0.04 (0.09)
Depression and anxiety	0.01	0.01 (0.08)	-0.05	-0.05 (0.09)	0.09	0.04 (0.09)	-0.07	-0.07 (0.08)	0.14	0.12 (0.09)
Mania and disorganization	-0.1	-0.12 (0.08)	-0.18	-0.17 (0.09)	0.07	0.07 (0.09)	-0.01	-0.02 (0.07)	-0.03	-0.05 (0.09)

eTable 7. Correlations Between the Individual Nonimaging Variables and the Imaging Variates for the Global and Modular Analyses in the Original Data Set (r) and Resampled Test-Sets (r^{TS})

	Global		**Cortical thickness**		**Subcortical volume**		**Task-based Activation**		**White Matter Fractional Anisotropy**	
Daily antipsychotic dose	-0.21	-0.22 (0.07)	-0.29	-0.26 (0.07)	0.13	0.14 (0.09)	-0.07	-0.07 (0.07)	-0.12	-0.08 (0.10)

r^{TS} = r of the resampled test-sets; SD=standard deviation; Females have higher values than males.

eTable 8. Global Analysis: Correlations Between the Individual Imaging Variables and the Nonimaging Variate in the Original Data Set (r) and the Resampled Test-Sets (r^{TS})

Region	Module	r-value	Mean r^{TS} (SD)
Left insula	Cortical Thickness	0.52	0.48 (0.07)
Right middle temporal gyrus	Cortical Thickness	0.50	0.47 (0.06)
Left lateral orbitofrontal cortex	Cortical Thickness	0.50	0.45 (0.07)
Left middle temporal gyrus	Cortical Thickness	0.50	0.47 (0.07)
Left precentral gyrus	Cortical Thickness	0.47	0.43 (0.07)
Right pars opercularis	Cortical Thickness	0.47	0.41 (0.07)
Right superior temporal gyrus	Cortical Thickness	0.47	0.43 (0.07)
Right fusiform	Cortical Thickness	0.46	0.45 (0.07)
Left posterior cingulate	Cortical Thickness	0.46	0.4 (0.08)
Right insula	Cortical Thickness	0.45	0.43 (0.07)
Left fusiform gyrus	Cortical Thickness	0.45	0.45 (0.08)
Right supramarginal	Cortical Thickness	0.43	0.39 (0.07)
Right inferior parietal	Cortical Thickness	0.43	0.38 (0.07)
Left supramarginal	Cortical Thickness	0.42	0.38 (0.07)
Right precuneus	Cortical Thickness	0.42	0.38 (0.07)
Left superior frontal gyrus	Cortical Thickness	0.41	0.33 (0.09)
Left pars triangularis	Cortical Thickness	0.41	0.36 (0.08)
Left pars opercularis	Cortical Thickness	0.40	0.35 (0.08)
Right posterior cingulate	Cortical Thickness	0.40	0.35 (0.09)
Left Posterior thalamic radiation	Fractional Anisotropy	0.40	0.36 (0.08)
Left superior temporal gyrus	Cortical Thickness	0.39	0.36 (0.07)
Right precentral gyrus	Cortical Thickness	0.39	0.34 (0.08)
Left inferior temporal gyrus	Cortical Thickness	0.39	0.37 (0.07)
RightPosterior thalamic radiation	Fractional Anisotropy	0.38	0.32 (0.09)

eTable 8. Global Analysis: Correlations Between the Individual Imaging Variables and the Nonimaging Variate in the Original Data Set (r) and the Resampled Test-Sets (r^{TS})

Region	Module	r-value	Mean r^{TS} (SD)
Left rostral middle frontal	Cortical Thickness	0.38	0.32 (0.08)
Right pars triangularis	Cortical Thickness	0.37	0.33 (0.07)
Right paracentral	Cortical Thickness	0.37	0.34 (0.08)
Right inferior temporal	Cortical Thickness	0.37	0.33 (0.07)
Left caudal middle frontal	Cortical Thickness	0.37	0.3 (0.08)
Right lateral orbitofrontal	Cortical Thickness	0.36	0.31 (0.08)
Right transverse temporal	Cortical Thickness	0.36	0.34 (0.07)
Left precuneus	Cortical Thickness	0.35	0.32 (0.07)
Right middle frontal	WM-task Activation	0.35	0.35 (0.07)
Right caudal middle frontal	Cortical Thickness	0.35	0.29 (0.08)
Left inferior parietal	Cortical Thickness	0.34	0.33 (0.07)
Right lateral occipital	Cortical Thickness	0.33	0.33 (0.08)
Right superior frontal	Cortical Thickness	0.33	0.26 (0.08)
Left lingual	Cortical Thickness	0.33	0.28 (0.08)
Right lingual	Cortical Thickness	0.32	0.29 (0.08)
Right inferior parietal lobule	WM-task Activation	0.32	0.31 (0.07)
Left temporal pole	Cortical Thickness	0.32	0.26 (0.09)
Left rostral anterior cingulate	Cortical Thickness	0.31	0.27 (0.07)
Left paracentral	Cortical Thickness	0.31	0.26 (0.09)
Left pars orbitalis	Cortical Thickness	0.31	0.27 (0.08)
Right postcentral	Cortical Thickness	0.31	0.28 (0.07)
Left middle frontal gyrus	WM-task Activation	0.31	0.31 (0.07)
Left transverse temporal	Cortical Thickness	0.31	0.28 (0.07)
Right pars orbitalis	Cortical Thickness	0.30	0.28 (0.07)

eTable 8. Global Analysis: Correlations Between the Individual Imaging Variables and the Nonimaging Variate in the Original Data Set (r) and the Resampled Test-Sets (r^{TS})

Region	Module	r-value	Mean r^{TS} (SD)
Right rostral middle frontal	Cortical Thickness	0.30	0.24 (0.08)
Right caudate	Subcortical Volume	0.29	0.23 (0.11)
Left medial orbitofrontal cortex	Cortical Thickness	0.29	0.25 (0.08)
Left inferior occipital gyrus	WM-task Activation	0.29	0.26 (0.08)
dorsal anterior cingulate cortex / SMA	WM-task Activation	0.28	0.29 (0.08)
FC within SAL	Resting-state FC	0.28	0.23 (0.08)
Genu of *corpus callosum*	Fractional Anisotropy	0.26	0.2 (0.09)
Left postcentral	Cortical Thickness	0.26	0.25 (0.07)
Right superior parietal	Cortical Thickness	0.26	0.23 (0.08)
Left lateral occipital	Cortical Thickness	0.26	0.26 (0.08)
Left caudate	Subcortical Volume	0.25	0.19 (0.1)
Left entorhinal cortex	Cortical Thickness	0.25	0.21 (0.08)
Right accumbens area	Subcortical Volume	0.25	0.21 (0.08)
Fornix	Fractional Anisotropy	0.25	0.22 (0.08)
Right inferior occipital gyrus	WM-task Activation	0.25	0.23 (0.07)
Left caudal anterior cingulate	Cortical Thickness	0.24	0.23 (0.09)
Left inferior parietal lobule	WM-task Activation	0.23	0.22 (0.07)
Body of corpus callosum	Fractional Anisotropy	0.22	0.2 (0.09)
Right entorhinal cortex	Cortical Thickness	0.22	0.19 (0.08)
Left lingual gyrus	WM-task Activation	0.22	0.19 (0.08)
Right putamen	Subcortical Volume	0.21	0.1 (0.13)
Left cerebellum cortex	Subcortical Volume	0.20	0.16 (0.08)
Right rostral anterior cingulate	Cortical Thickness	0.20	0.19 (0.08)
Right anterior corona radiata	Fractional Anisotropy	0.19	0.16 (0.09)

eTable 8. Global Analysis: Correlations Between the Individual Imaging Variables and the Nonimaging Variate in the Original Data Set (r) and the Resampled Test-Sets (r^{TS})

Region	Module	r-value	Mean r^{TS} (SD)
Left superior parietal	Cortical Thickness	0.19	0.17 (0.07)
Right middle temporal gyrus	WM-task Activation	0.18	0.15 (0.07)
Right hippocampus	Subcortical Volume	0.18	0.18 (0.09)
Left anterior corona radiata	Fractional Anisotropy	0.18	0.13 (0.09)
Left hippocampus	Subcortical Volume	0.18	0.17 (0.09)
Right superior longitudinal fasciculus	Fractional Anisotropy	0.18	0.14 (0.09)
Left superior longitudinal fasciculus	Fractional Anisotropy	0.18	0.14 (0.08)
Left thalamus	Subcortical Volume	0.17	0.17 (0.08)
Left putamen	Subcortical Volume	0.17	0.07 (0.12)
Right temporal pole	Cortical Thickness	0.17	0.15 (0.08)
Right parahippocampal	Subcortical Volume	0.17	0.17 (0.07)
FC between CEN and AUD	Resting-state FC	0.17	0.14 (0.08)
Right corona radiata	Fractional Anisotropy	0.17	0.12 (0.09)
Right middle frontal gyrus	ER-task Activation	0.17	0.12 (0.09)
Dorsal anterior cingulate cortex	WM-task Activation	0.16	0.16 (0.08)
Left amygdala	Subcortical Volume	0.16	0.16 (0.08)
Right fornix (cres) / *Stria terminalis*	Fractional Anisotropy	0.16	0.21 (0.09)
Left fornix (cres) / *Stria terminalis*	Fractional Anisotropy	0.16	0.18 (0.09)
Right cerebellum cortex	Subcortical Volume	0.15	0.12 (0.08)
Right inferior occipital gyrus	ER-task Activation	0.14	0.13 (0.08)
Right caudal anterior cingulate	Cortical Thickness	0.14	0.13 (0.08)
Left corona radiata	Fractional Anisotropy	0.14	0.09 (0.09)
Right inferior fronto-occipital fasciculus	Fractional Anisotropy	0.14	0.12 (0.09)
Right thalamus	Subcortical Volume	0.14	0.12 (0.08)

eTable 8. Global Analysis: Correlations Between the Individual Imaging Variables and the Nonimaging Variate in the Original Data Set (r) and the Resampled Test-Sets (r^{TS})

Region	Module	r-value	Mean r^{TS} (SD)
Right cuneus	Cortical Thickness	0.14	0.13 (0.08)
Left cuneus	Cortical Thickness	0.14	0.09 (0.07)
Splenium of corpus callosum	Fractional Anisotropy	0.14	0.11 (0.08)
Left External capsule	Fractional Anisotropy	0.14	0.11 (0.08)
Right medial orbitofrontal	Cortical Thickness	0.13	0.13 (0.08)
Right anterior limb of internal capsule	Fractional Anisotropy	0.13	0.11 (0.09)
Left frontal pole	Cortical Thickness	0.13	0.12 (0.08)
Right external capsule	Fractional Anisotropy	0.12	0.11 (0.09)
Left inferior occipital gyrus	ER-task Activation	0.12	0.09 (0.07)
Left inferior fronto-occipital fasciculus	Fractional Anisotropy	0.12	0.1 (0.08)
Right frontal pole	Cortical Thickness	0.12	0.11 (0.08)
Left anterior limb of internal capsule	Fractional Anisotropy	0.12	0.11 (0.09)
Right superior temporal gyrus	ER-task Activation	0.11	0.09 (0.1)
Posterior corona radiata	Fractional Anisotropy	0.11	0.07 (0.08)
FC between DMN and SAL	Resting-state FC	0.11	0.15 (0.09)
Right pallidum	Subcortical Volume	0.11	0.02 (0.11)
Right internal capsule	Fractional Anisotropy	0.10	0.06 (0.08)
FC within VIS	Resting-state FC	0.10	0.09 (0.08)
FC within DMN	Resting-state FC	0.09	0.1 (0.08)
FC between DMN and VIS	Resting-state FC	0.09	0.08 (0.09)
Left pericalcarine	Cortical Thickness	0.09	0.03 (0.1)
Left accumbens area	Subcortical Volume	0.09	0.03 (0.09)
Right middle temporal gyrus	WM-task Activation	0.07	0.08 (0.07)
Right superior corona radiata	Fractional Anisotropy	0.07	0.04 (0.09)

eTable 8. Global Analysis: Correlations Between the Individual Imaging Variables and the Nonimaging Variate in the Original Data Set (r) and the Resampled Test-Sets (r^{TS})

Region	Module	r-value	Mean r^{TS} (SD)
Left parahippocampal	Cortical Thickness	0.07	0.05 (0.08)
Right amygdala	Subcortical Volume	0.06	0.05 (0.08)
Right Retrolenticular part of internal capsule	Fractional Anisotropy	0.06	0.04 (0.08)
Left Retrolenticular part of internal capsule	Fractional Anisotropy	0.06	0.03 (0.08)
Right Cingulum (hippocampal portion)	Fractional Anisotropy	0.06	0.07 (0.08)
Left middle frontal gyrus	ER-task Activation	0.05	0.03 (0.07)
Left Superior corona radiata	Fractional Anisotropy	0.05	0.02 (0.09)
Right Posterior limb of internal capsule	Fractional Anisotropy	0.05	0.01 (0.08)
Right Posterior *corona radiata*	Fractional Anisotropy	0.05	0.01 (0.09)
Right Superior fronto-occipital fasciculus	Fractional Anisotropy	0.04	0.03 (0.1)
Right pericalcarine	Cortical Thickness	0.04	0.03 (0.08)
Left Cingulum (hippocampal portion)	Fractional Anisotropy	0.04	0.08 (0.09)
Right fusiform gyrus	ER-task Activation	0.03	0 (0.08)
Left inferior frontal gyrus	ER-task Activation	0.03	0.03 (0.06)
Left pallidum	Subcortical Volume	0.03	-0.04 (0.1)
FC between SAL and VIS	Resting-state FC	0.03	0.01 (0.08)
Left Internal capsule	Fractional Anisotropy	0.02	0 (0.08)
FC between DMN and AUD	Resting-state FC	0.02	0.01 (0.09)
FC between CEN and SMN	Resting-state FC	0.02	0.02 (0.08)
FC within AUD	Resting-state FC	0.02	0.02 (0.09)
Left Superior fronto-occipital fasciculus	Fractional Anisotropy	0.02	0.02 (0.09)

eTable 8. Global Analysis: Correlations Between the Individual Imaging Variables and the Nonimaging Variate in the Original Data Set (r) and the Resampled Test-Sets (r^{TS})

Region	Module	r-value	Mean r^{TS} (SD)
Left middle temporal gyrus	WM-task Activation	0.02	0 (0.08)
Right amygdala	ER-task Activation	0.01	-0.02 (0.08)
FC between VIS and SMN	Resting-state FC	0.01	0.03 (0.07)
Right inferior frontal gyrus	ER-task Activation	0.01	0 (0.07)
Left cuneus	ER-task Activation	0.01	0.02 (0.07)
FC between CEN and VIS	Resting-state FC	0.00	-0.01 (0.08)
Left Cingulum	Fractional Anisotropy	0.00	0 (0.09)
FC within CEN	Resting-state FC	0.00	0.01 (0.07)
FC between AUD and VIS	Resting-state FC	0.00	0.03 (0.09)
Right Uncinate fasciculus	Fractional Anisotropy	0.00	-0.01 (0.07)
Right Cingulum (cingulate gyrus)	Fractional Anisotropy	0.00	-0.02 (0.09)
Left fusiform gyrus	ER-task Activation	-0.03	-0.07 (0.08)
Left amygdala	ER-task Activation	-0.03	-0.06 (0.09)
FC within SMN	Resting-state FC	-0.03	-0.01 (0.08)
FC between DMN and SMN	Resting-state FC	-0.04	-0.02 (0.09)
FC between SAL and SMN	Resting-state FC	-0.05	-0.06 (0.09)
Left uncinate fasciculus	Fractional Anisotropy	-0.07	-0.1 (0.09)
Precuneus	ER-task Activation	-0.08	-0.06 (0.07)
Right cuneus	ER-task Activation	-0.08	-0.08 (0.07)
FC between SAL and AUD	Resting-state FC	-0.09	-0.09 (0.09)

r^{TS} = r of the 5000 resampled test-sets; SD=standard deviation; AUD = auditory network, CEN = central executive network, DMN = default mode network, ER = emotion recognition task (faces vs shapes contrast), SAL = salience network, SMA = Supplementary Motor Area; SMN = sensorimotor network, VIS = visual network, WM = working memory task (2-back vs 0-back contrast); FC=functional connectivity

eTable 9. Cortical Thickness Module: Correlations Between the Individual Cortical Thickness Variables and the Nonimaging Variate in the Original Data Set (r) and Resampled Test-Sets (r^{TS})

Region	r-value	Mean r^{TS} (SD)
Left middle temporal gyrus	0.54	0.48 (0.07)
Left insula	0.54	0.47 (0.07)
Right middle temporal gyrus	0.54	0.48 (0.07)
Right fusiform gyrus	0.52	0.49 (0.07)
Left fusiform gyrus	0.52	0.47 (0.08)
Left lateral orbitofrontal cortex	0.51	0.44 (0.08)
Right superior temporal gyrus	0.50	0.45 (0.07)
Left precentral gyrus	0.50	0.44 (0.07)
Right insula	0.50	0.44 (0.07)
Right pars opercularis	0.47	0.42 (0.07)
Left posterior cingulate	0.46	0.4 (0.08)
Left inferior temporal gyrus	0.45	0.4 (0.07)
Right supramarginal	0.44	0.39 (0.07)
Left superior temporal gyrus	0.44	0.39 (0.07)
Right inferior parietal	0.44	0.38 (0.08)
Left supramarginal	0.44	0.39 (0.07)
Right precuneus	0.43	0.37 (0.07)
Left pars triangularis	0.40	0.35 (0.09)
Right precentral gyrus	0.40	0.34 (0.08)
Right posterior cingulate	0.40	0.34 (0.09)
Right transverse temporal	0.39	0.36 (0.07)
Left pars opercularis	0.39	0.33 (0.08)
Right paracentral	0.39	0.34 (0.08)
Right lateral occipital lobe	0.38	0.36 (0.08)

eTable 9. Cortical Thickness Module: Correlations Between the Individual Cortical Thickness Variables and the Nonimaging Variate in the Original Data Set (r) and Resampled Test-Sets (r^{TS})

Region	r-value	Mean r^{TS} (SD)
Left inferior parietal	0.38	0.34 (0.07)
Left superior frontal gyrus	0.38	0.32 (0.09)
Left rostral middle frontal	0.38	0.31 (0.08)
Right inferior temporal gyrus	0.38	0.33 (0.07)
Right pars triangularis	0.37	0.33 (0.08)
Left precuneus	0.37	0.32 (0.08)
Right lateral orbitofrontal	0.36	0.3 (0.08)
Right lingual gyrus	0.36	0.31 (0.08)
Left caudal middle frontal	0.35	0.29 (0.09)
Right caudal middle frontal	0.34	0.29 (0.09)
Left transversetemporal	0.33	0.29 (0.07)
Left lingual gyrus	0.33	0.28 (0.08)
Right postcentral gyrus	0.33	0.29 (0.07)
Left temporal pole	0.32	0.25 (0.09)
Right pars orbitalis	0.32	0.28 (0.07)
Left lateral occipital lobe	0.31	0.29 (0.08)
Right superior frontal gyrus	0.31	0.26 (0.09)
Left pars orbitalis	0.31	0.26 (0.08)
Left paracentral	0.30	0.26 (0.09)
Left postcentral gyrus	0.30	0.27 (0.07)
Left rostral anterior cingulate	0.30	0.25 (0.08)
Right rostral middle frontal	0.29	0.24 (0.08)
Left medial orbitofrontal cortex	0.28	0.23 (0.08)
Left caudal anterior cingulate	0.27	0.24 (0.09)

eTable 9. Cortical Thickness Module: Correlations Between the Individual Cortical Thickness Variables and the Nonimaging Variate in the Original Data Set (r) and Resampled Test-Sets (r^{TS})

Region	r-value	Mean r^{TS} (SD)
Right superior parietal	0.27	0.23 (0.08)
Left entorhinal cortex	0.24	0.2 (0.09)

r^{TS} = r of the 5000 resampled test-sets; SD=standard deviation

eTable 10. Subcortical Volume Module: Correlations Between the Individual Subcortical Volume Variables and the Nonimaging Variate in the Original Data Set (r) and Resampled Test-Sets (r^{TS})

Region	r-value	Mean r^{TS} (SD)
Left Caudate	0.39	0.26 (0.11)
Left Thalamus	0.37	0.11 (0.15)
Right Caudate	0.36	0.24 (0.12)
Left Pallidum	0.31	0.22 (0.11)
Right Putamen	0.29	0.27 (0.1)
Right Thalamus	0.29	0.11 (0.12)
Left Accumbens area	0.27	0.16 (0.11)
Right Accumbens area	0.23	0.13 (0.11)
Right Pallidum	0.21	0.21 (0.09)
Left Putamen	0.20	0.22 (0.1)
Right Hippocampus	0.08	0 (0.13)
Left Hippocampus	0.06	-0.01 (0.13)
Right Cerebellum Cortex	-0.06	-0.01 (0.12)
Left Cerebellum Cortex	-0.10	-0.02 (0.14)
Left Amygdala	-0.11	-0.06 (0.14)
Right Amygdala	-0.11	-0.03 (0.1)
Right lateral Ventricle	-0.17	-0.08 (0.11)
Left lateral Ventricle	-0.19	-0.08 (0.12)

r^{TS} = r of the 5000 resampled test-sets; SD=standard deviation

eTable 11. Task Activation Module: Correlations Between the Individual Task-Related Brain Activation Variables and the Nonimaging Variate in the Original Data Set (r) and Resampled Test-Sets (r^{TS})

Task and Region	r-value	Mean r^{TS} (SD)
Right WM middle frontal gyrus	0.38	0.3 (0.1)
Left WM middle frontal gyrus	0.37	0.3 (0.09)
Right WM inferior parietal lobule	0.35	0.27 (0.09)
WM dorsal anterior cingulate cortex / SMA	0.34	0.25 (0.1)
Left WM inferior occipital gyrus	0.28	0.19 (0.11)
Left WM inferior parietal lobule	0.26	0.2 (0.09)
Right WM inferior occipital gyrus	0.26	0.19 (0.08)
Right ER inferior occipital gyrus	0.21	0.14 (0.09)
Left WM lingual gyrus	0.20	0.13 (0.09)
WM dorsal anterior cingulate cortex	0.19	0.14 (0.08)
Right WM middle temporal gyrus	0.18	0.11 (0.09)
Left ER inferior occipital gyrus	0.17	0.11 (0.08)
Right ER superior temporal gyrus	0.11	0.07 (0.09)
Right WM middle temporal gyrus	0.10	0.04 (0.08)
Right ER middle frontal gyrus	0.10	0.03 (0.1)
Left ER inferior frontal gyrus	0.06	0.05 (0.07)
ER Left middle frontal gyrus	0.04	0.01 (0.08)
Left ER cuneus	0.03	0.03 (0.08)
Left WM middle temporal gyrus	0.00	-0.01 (0.08)
Right ER fusiform gyrus	0.00	-0.01 (0.08)
Right ER inferior frontal gyrus	-0.01	0.01 (0.08)
Right ER amygdala	-0.02	-0.03 (0.08)
ER Precuneus	-0.05	-0.03 (0.08)
Left ER amygdala	-0.06	-0.07 (0.1)

Left ER fusiform gyrus	-0.07	-0.1 (0.09)
Right ER cuneus	-0.08	-0.06 (0.08)

ER = Emotion Recognition task (emotional faces > shapes contrast); WM = Working Memory task (2-back > 0-back contrast); r^{TS} = r of the 5000 resampled test-sets; SD=standard deviation

eTable 12. White Matter Fractional Anisotropy Module: Correlations Between the Individual Fractional Anisotropy Variables With the Nonimaging Variate in the Original Data Set (r) and Resampled Test-Sets (r^{TS})

Tracks	r-value	Mean r-value^{TS} (SD)
Left Posterior thalamic radiation	0.43	0.29 (0.11)
Right Posterior thalamic radiation	0.38	0.23 (0.12)
Fornix	0.27	0.17 (0.09)
Body of *corpus callosum*	0.25	0.14 (0.1)
Genu of *corpus callosum*	0.24	0.12 (0.12)
Right Fornix (cres) / *Stria terminalis*	0.22	0.19 (0.11)
Right Superior longitudinal fasciculus	0.20	0.09 (0.1)
Left Superior longitudinal fasciculus	0.19	0.1 (0.1)
Left Fornix (cres) / *Stria terminalis*	0.19	0.14 (0.1)
Right Anterior *corona radiata*	0.17	0.08 (0.09)
Splenium of *corpus callosum*	0.16	0.08 (0.1)
Right Corona radiata	0.16	0.07 (0.09)
Right Inferior fronto-occipital fasciculus	0.16	0.1 (0.11)
Right Anterior limb of internal capsule	0.15	0.09 (0.1)
Right External capsule	0.14	0.08 (0.09)
Left Anterior corona radiata	0.13	0.05 (0.09)
Posterior *corona radiata*	0.13	0.05 (0.09)
Left External capsule	0.13	0.06 (0.1)
Left Anterior limb of internal capsule	0.11	0.06 (0.09)
Left Corona radiata	0.11	0.02 (0.09)
Right Internal capsule	0.10	0.03 (0.09)
Right Cingulum (hippocampal portion)	0.10	0.06 (0.09)
Left Cingulum (hippocampal portion)	0.10	0.09 (0.12)
Left Inferior fronto-occipital fasciculus	0.09	0.05 (0.09)

Right Retrolenticular part of internal capsule	0.07	0.02 (0.1)
Right Superior *corona radiata*	0.07	0.01 (0.1)
Right Superior fronto-occipital fasciculus	0.06	0.01 (0.1)
Left Retrolenticular part of internal capsule	0.05	-0.01 (0.09)
Right Posterior *corona radiata*	0.05	0 (0.09)
Left Superior corona radiata	0.04	-0.01 (0.09)
Right Uncinate fasciculus	0.03	0 (0.09)
Left Superior fronto-occipital fasciculus	0.02	0 (0.09)
Right Posterior limb of internal capsule	0.02	-0.03 (0.1)
Left Internal capsule	0.01	-0.03 (0.08)
Left Cingulum	0.01	-0.02 (0.1)
Right Cingulum	0.01	-0.05 (0.09)
Left Uncinate fasciculus	-0.07	-0.1 (0.1)
Left Posterior limb of internal capsule	-0.13	-0.12 (0.09)

r^{TS} = r of the 5000 resampled test-sets; SD=standard deviation

eFigures. Supplemental Figures

eFigure 1. Case-Control Differences in Cortical Thickness. Items marked with * are significant at p<0.05, FDR corrected; HV=healthy volunteers

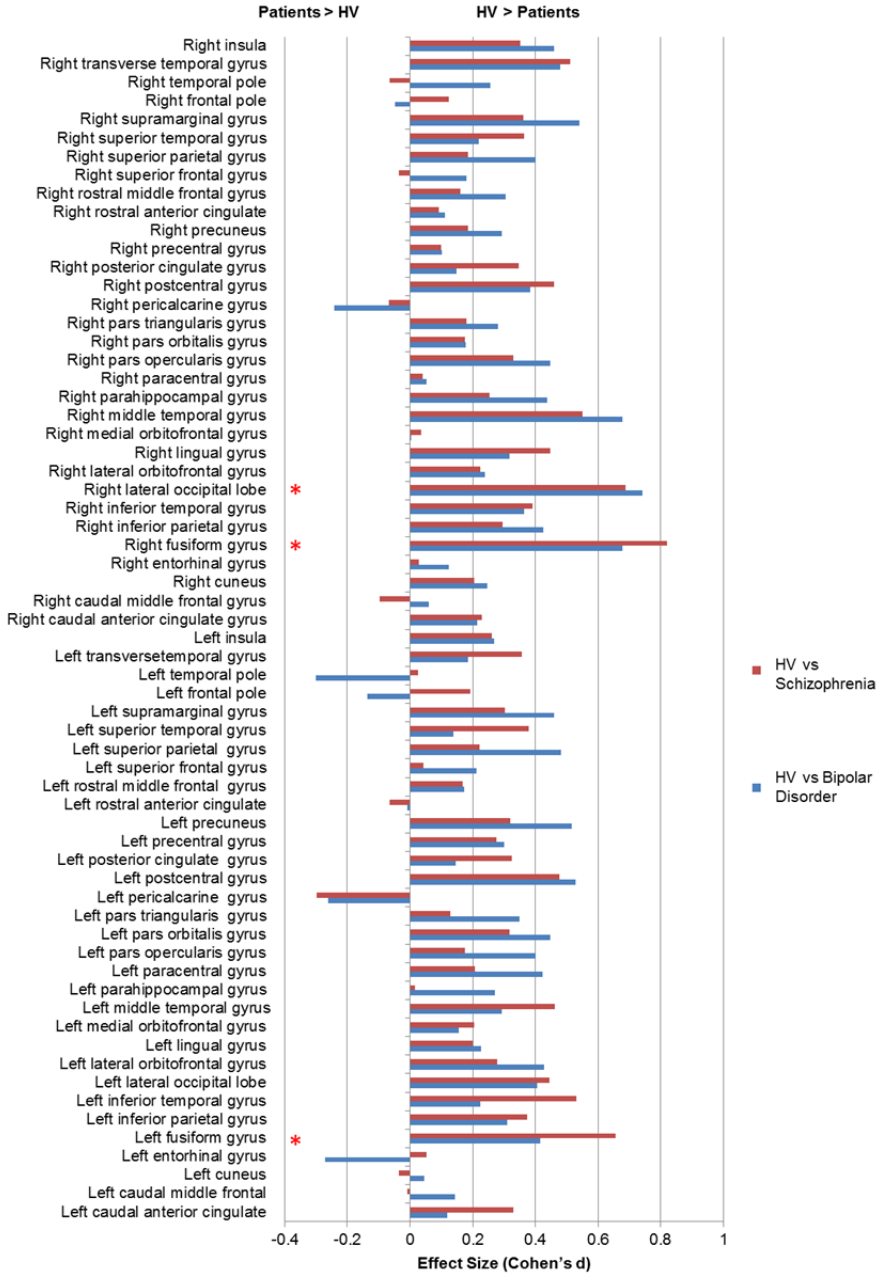

eFigure 2. Case-Control Differences in Subcortical Volumes. Items marked with * are significant at p<0.05, FDR corrected; HV=Healthy volunteers

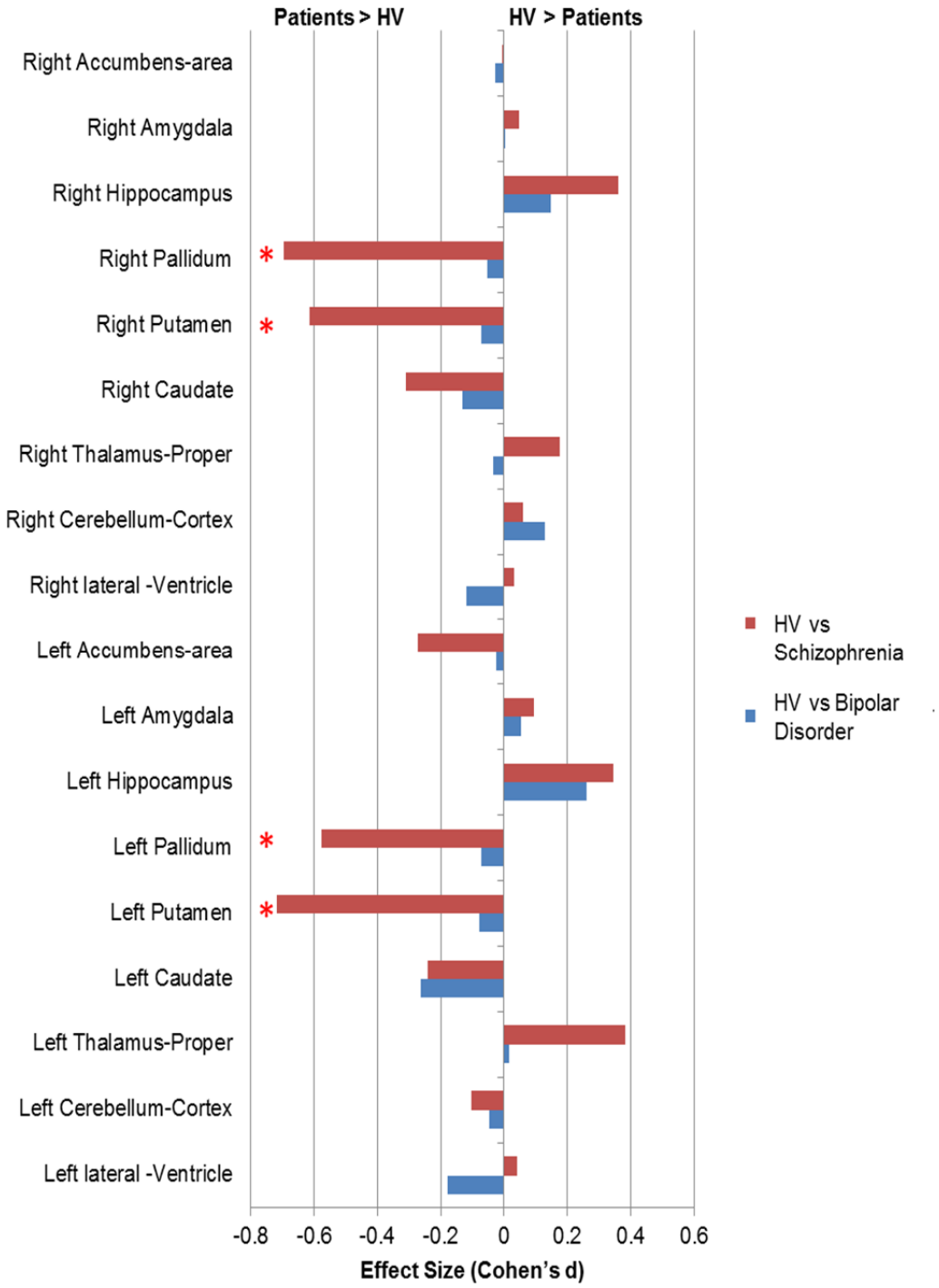

eFigure 3. Case-Control Differences in Fractional Anisotropy Measures. Items marked with * are significant at p<0.05, FDR corrected; HV=Healthy volunteers

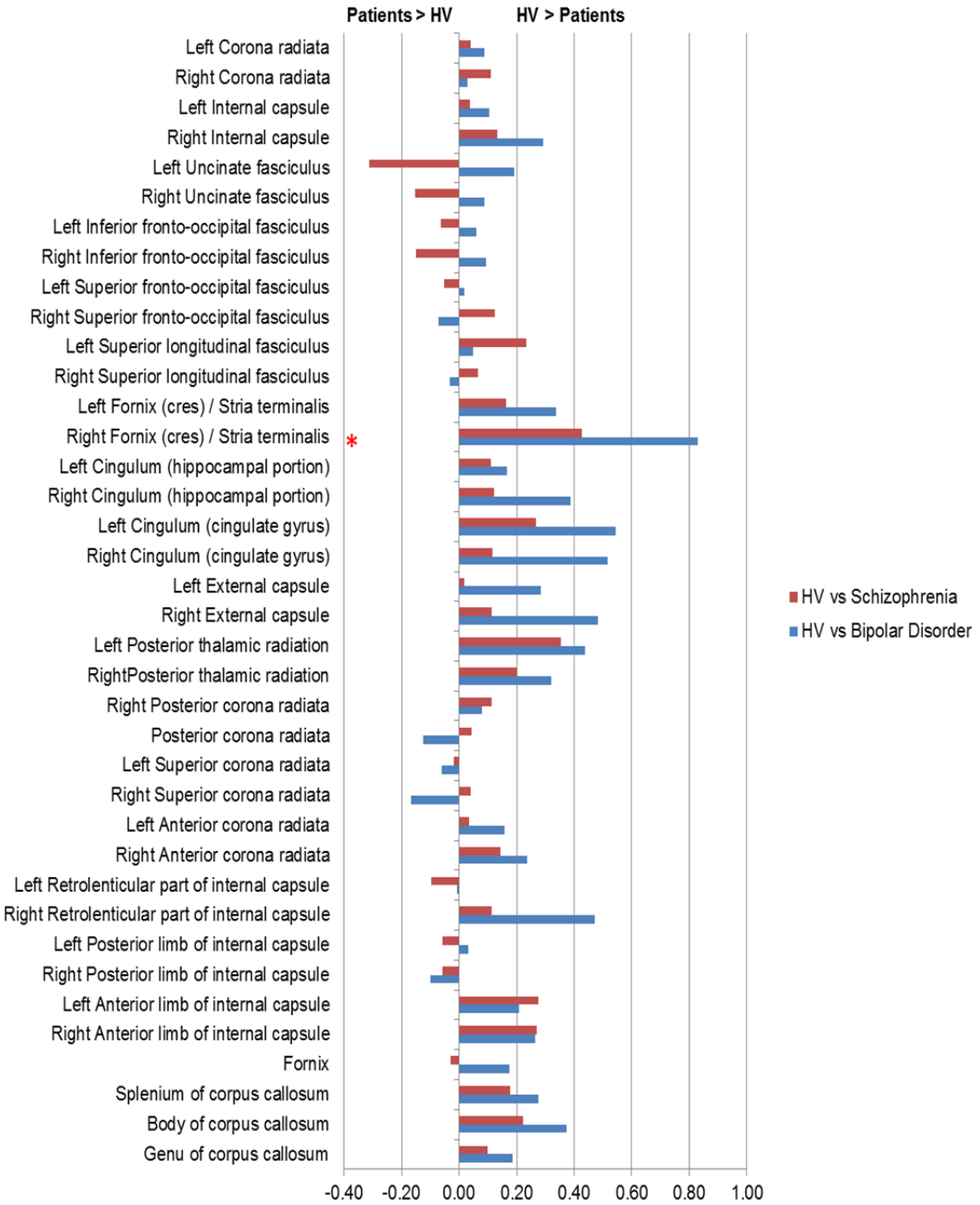

eFigure 4. Case-Control Differences in Resting-State Functional Connectivity. Items marked with * are significant at p<0.05, FDR corrected. Effect size for the resting-state functional connectivity measures between healthy volunteers (HV) and patients with either bipolar disorder (blue) or schizophrenia (red). Abbreviations: BN-FC: Between-network functional connectivity, WN-FC: within-network functional connectivity, AUD: auditory network, DMN: Default-mode network, ECN: Executive central network, SAL: Salience network, SMN: Sensorimotor network, VIS: visual network.

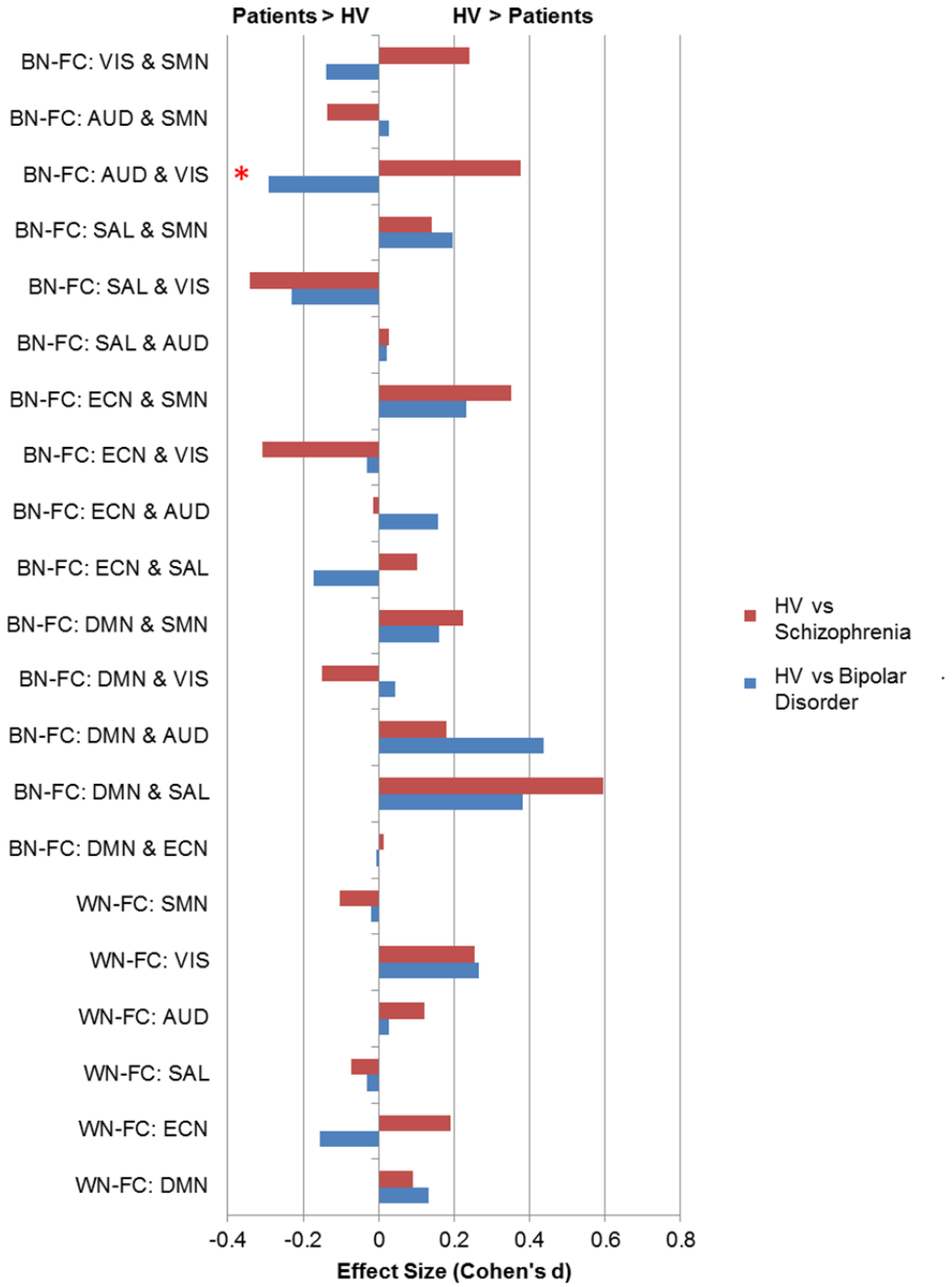

eFigure 5. Activation Patterns Associated With the fMRI Tasks in the Study and Human Connectome Project (HCP) Samples. (A) working memory task; (B) emotion recognition task.

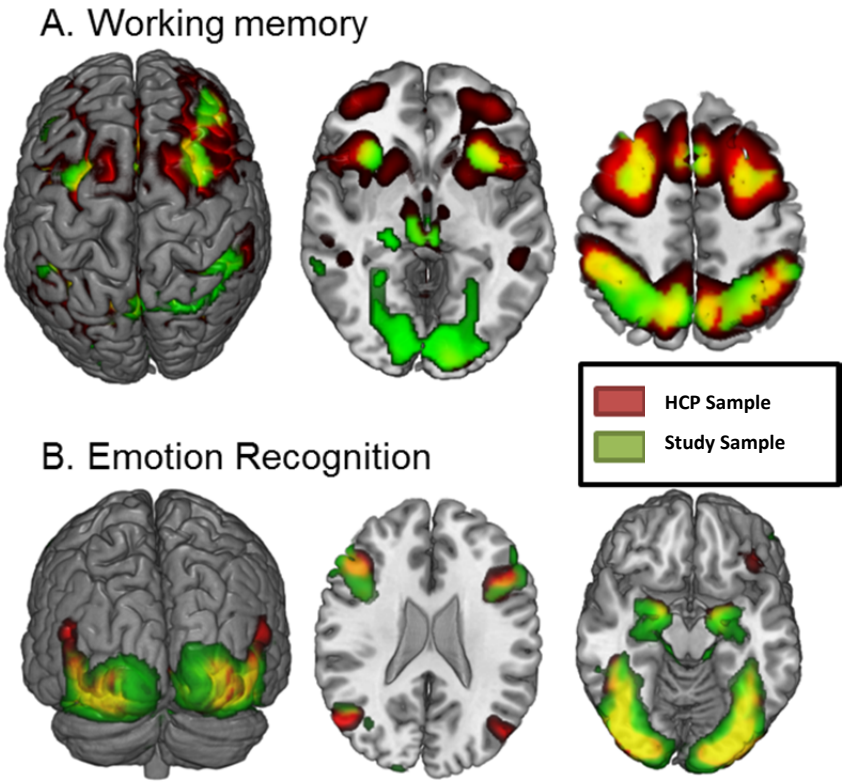

eFigure 6. Resting-State Networks

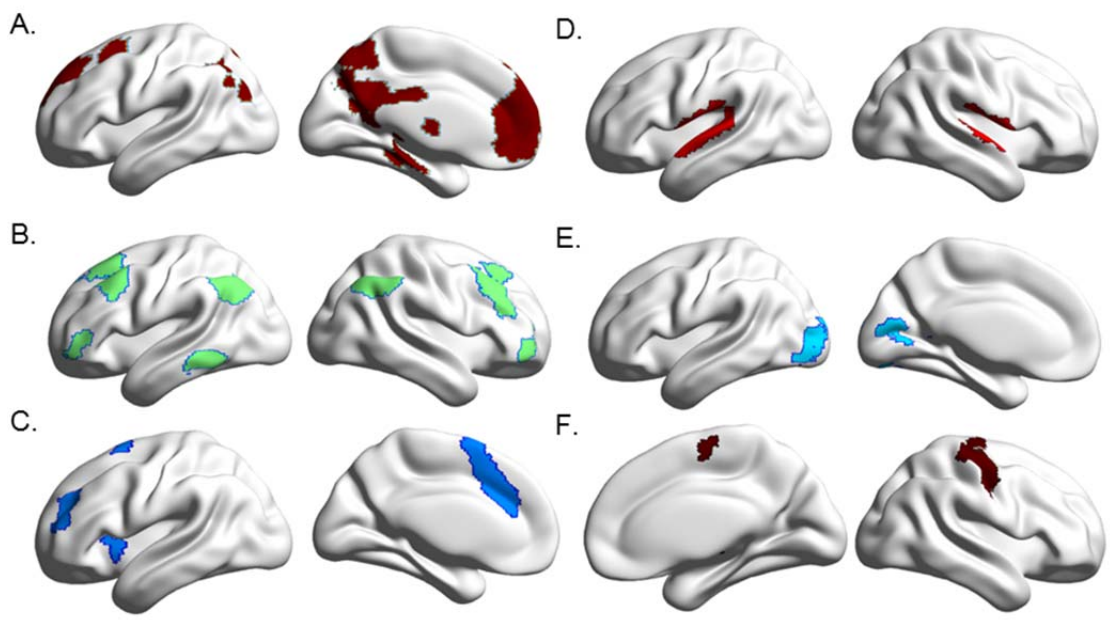

(A) Default Mode network (B) Central Executive Network (C) Salience Network (D) Auditory Network (E) Visual Network (F) Sensorimotor network

eFigure 7. Manhattan Plots of Univariate Correlations Between Imaging and Nonimaging Variables. The y-axis shows the (negative) logarithm of the significance (p-value). (A) Plots of the non-imaging variables (all are age-regressed, except *age itself); (B) Plots of the neuroimaging variables per imaging mode. In Panel B only, age-adjusted values are in color while unadjusted values are in gray.

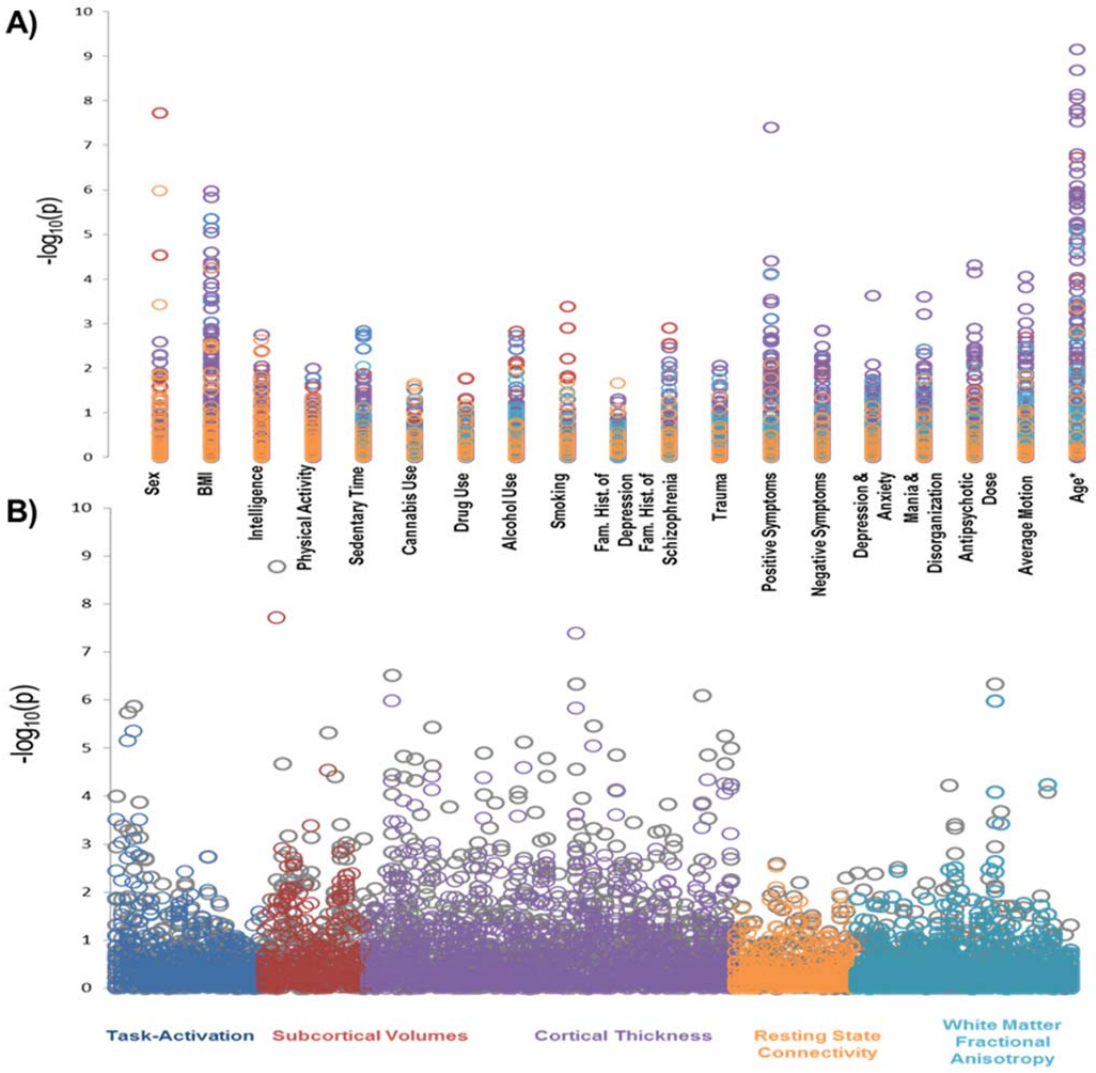

eFigure 8. Histogram of the Redundancy-Reliability Score (RR-Scores) of the Global and Modular sCCAs. Presented is the information for the first three canonical modes.

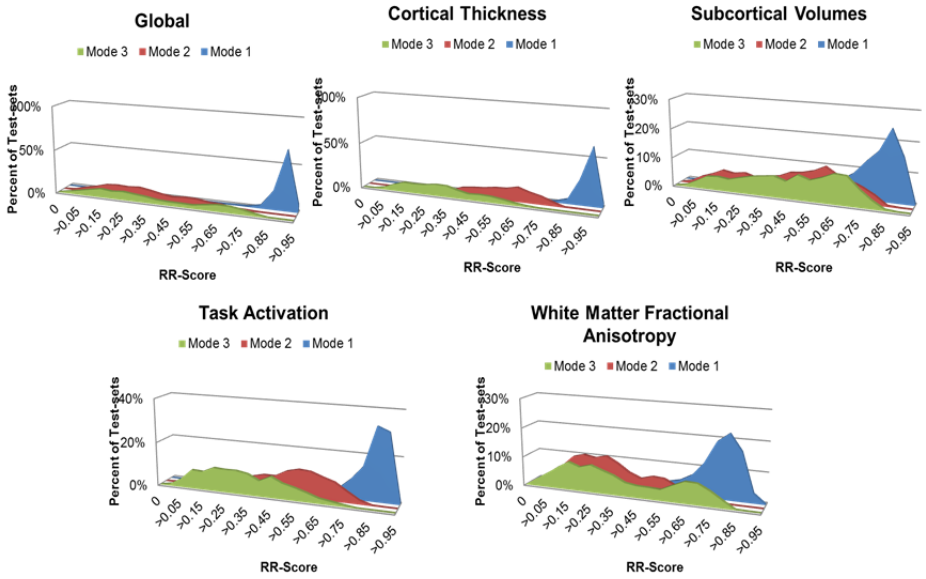

eFigure 9. Effect of Sample Size on sCCA Correlations. All confidence intervals at 95% are below 0.005.

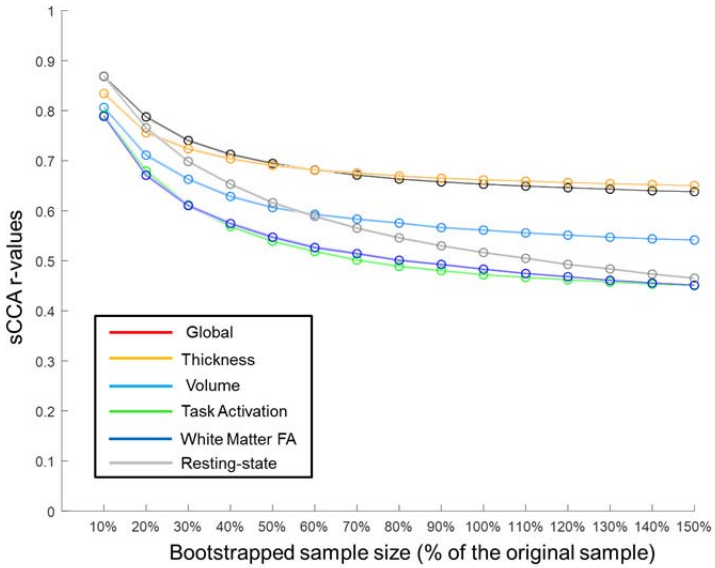

eFigure 10.1. Scatterplots for Each Modular sCCA, by Diagnostic Group

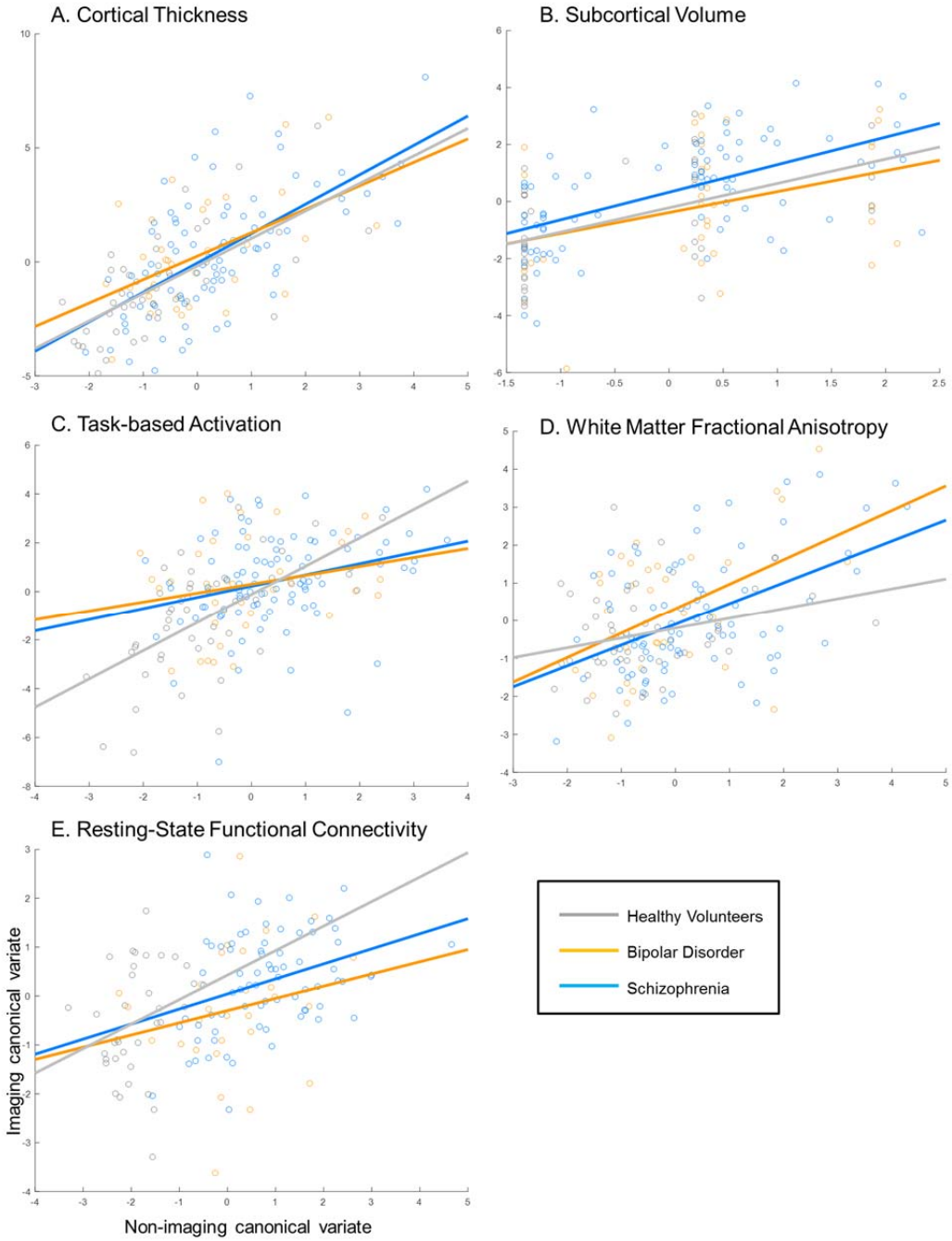

eFigure 10.2. Scatterplots for Each sCCA, for Healthy Volunteers vs Patients. Patients with bipolar disorder and patients with schizophrenia were collapsed into a single group.

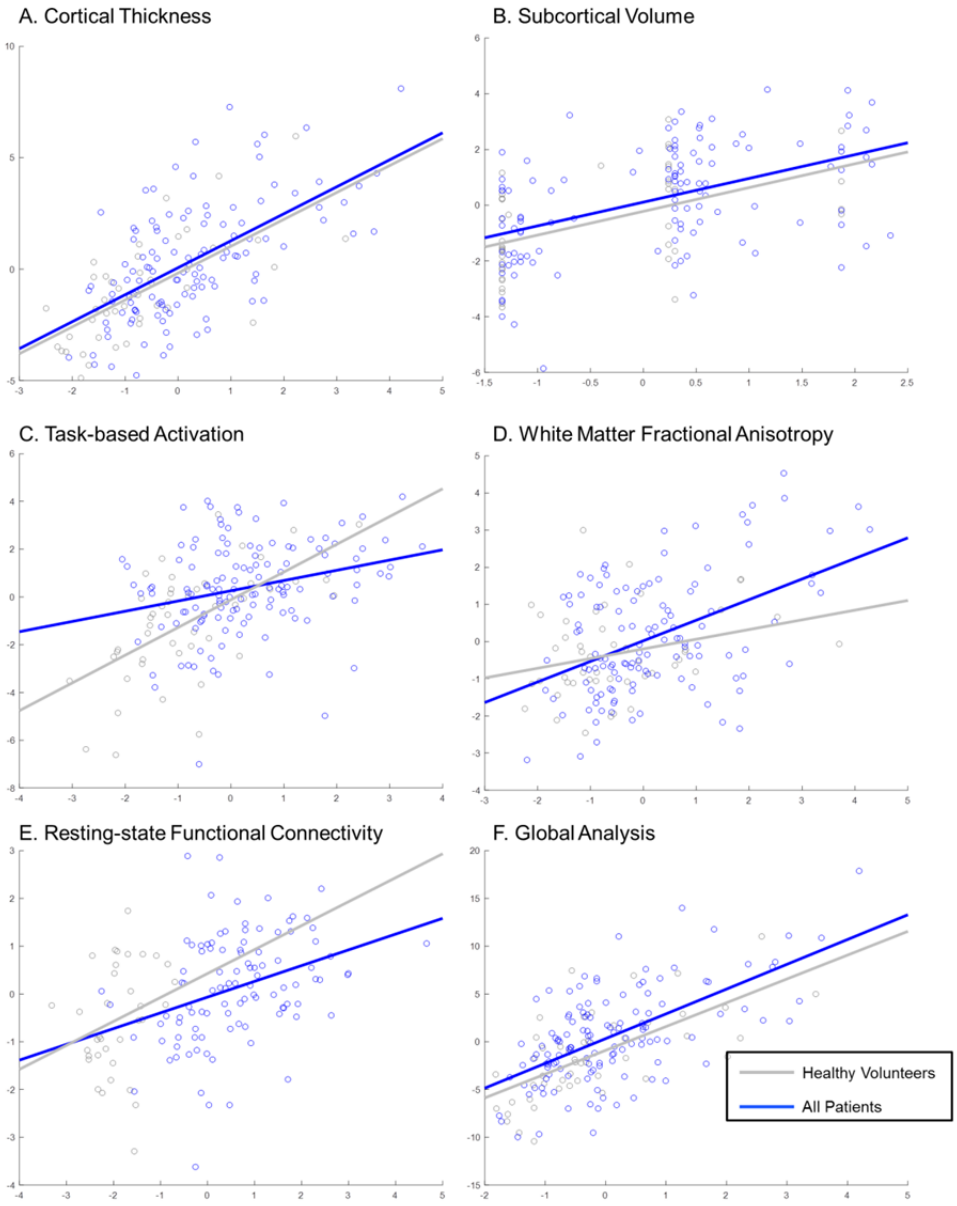

eFigure 11. Results of the sCCAs Top Nonimaging Variables, Computed for Each Diagnostic Group. Correlations of top 5 non-imaging variables with the imaging variate resulting from separate sCCAs for each diagnostic group. Abbreviations: BD = Bipolar Disorder, HV =Healthy Volunteers, SCZ= Schizophrenia.

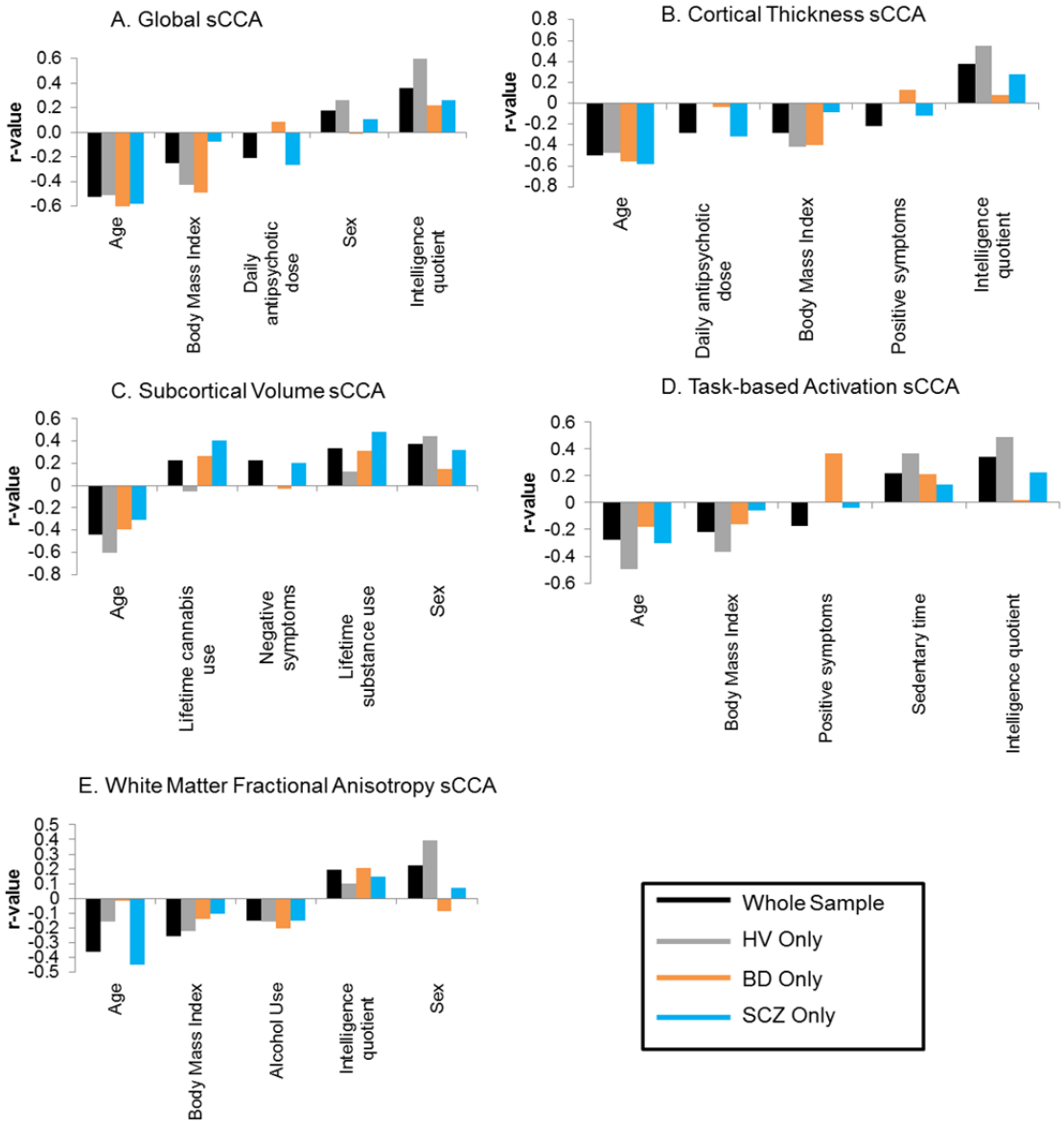

eFigure 12. Reliability of the Top Nonimaging Variables. The mean r^{TS} value is shown as black-filled circles and the standard deviation is depicted as a shaded area. The colored lines/circles show the r-value for each sCCA of the actual data.

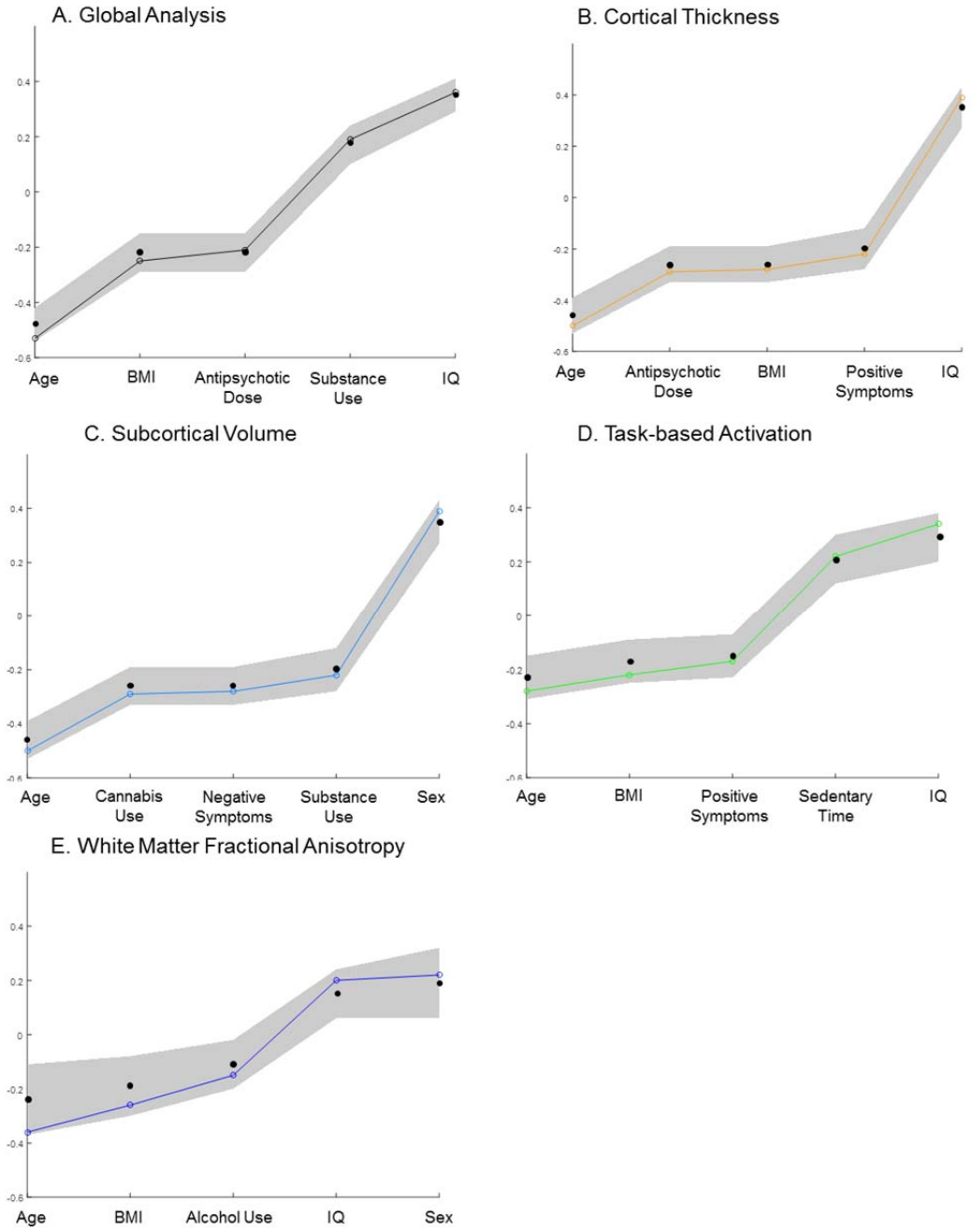

eReferences

1. Association AP. *Diagnostic and statistical manual of mental disorders.* Arlington, VA: American Psychiatric Publishing; 2013.
2. First MB, Williams JBW, Karg RS, Spitzer RL. *Structured clinical interview for DSM-5, research version.* Arlington, VA2015.
3. Segonne F, Dale AM, Busa E, et al. A hybrid approach to the skull stripping problem in MRI. *Neuroimage.* 2004;22(3):1060-1075.
4. Fischl B, Salat DH, Busa E, et al. Whole brain segmentation: automated labeling of neuroanatomical structures in the human brain. *Neuron.* 2002;33(3):341-355.
5. Fischl B, Salat DH, van der Kouwe AJ, et al. Sequence-independent segmentation of magnetic resonance images. *Neuroimage.* 2004;23 Suppl 1:S69-84.
6. Sled JG, Zijdenbos AP, Evans AC. A nonparametric method for automatic correction of intensity nonuniformity in MRI data. *IEEE Trans Med Imaging.* 1998;17(1):87-97.
7. Fischl B, Liu A, Dale AM. Automated manifold surgery: constructing geometrically accurate and topologically correct models of the human cerebral cortex. *IEEE Trans Med Imaging.* 2001;20(1):70-80.
8. Segonne F, Pacheco J, Fischl B. Geometrically accurate topology-correction of cortical surfaces using nonseparating loops. *IEEE Trans Med Imaging.* 2007;26(4):518-529.
9. Fischl B, Dale AM. Measuring the thickness of the human cerebral cortex from magnetic resonance images. *Proc Natl Acad Sci U S A.* 2000;97(20):11050-11055.
10. Pintzka CW, Hansen TI, Evensmoen HR, Haberg AK. Marked effects of intracranial volume correction methods on sex differences in neuroanatomical structures: a HUNT MRI study. *Front Neurosci.* 2015;9:238.
11. Glasser MF, Sotiropoulos SN, Wilson JA, et al. The minimal preprocessing pipelines for the Human Connectome Project. *Neuroimage.* 2013;80:105-124.
12. Smith SM, Jenkinson M, Johansen-Berg H, et al. Tract-based spatial statistics: voxelwise analysis of multi-subject diffusion data. *Neuroimage.* 2006;31(4):1487-1505.
13. Mori S, Oishi K, Jiang H, et al. Stereotaxic white matter atlas based on diffusion tensor imaging in an ICBM template. *Neuroimage.* 2008;40(2):570-582.
14. Kelly S, Jahanshad N, Zalesky A, et al. Widespread white matter microstructural differences in schizophrenia across 4322 individuals: results from the ENIGMA Schizophrenia DTI Working Group. *Mol Psychiatry.* 2017.
15. Yan CG, Wang XD, Zuo XN, Zang YF. DPABI: Data Processing & Analysis for (Resting-State) Brain Imaging. *Neuroinformatics.* 2016;14(3):339-351.
16. Patel AX, Kundu P, Rubinov M, et al. A wavelet method for modeling and despiking motion artifacts from resting-state fMRI time series. *Neuroimage.* 2014;95:287-304.
17. Friston KJ, Williams S, Howard R, Frackowiak RS, Turner R. Movement-related effects in fMRI time-series. *Magn Reson Med.* 1996;35(3):346-355.
18. Behzadi Y, Restom K, Liau J, Liu TT. A component based noise correction method (CompCor) for BOLD and perfusion based fMRI. *Neuroimage.* 2007;37(1):90-101.
19. Power JD, Barnes KA, Snyder AZ, Schlaggar BL, Petersen SE. Spurious but systematic correlations in functional connectivity MRI networks arise from subject motion. *Neuroimage.* 2012;59(3):2142-2154.
20. Power JD, Mitra A, Laumann TO, Snyder AZ, Schlaggar BL, Petersen SE. Methods to detect, characterize, and remove motion artifact in resting state fMRI. *Neuroimage.* 2014;84:320-341.
21. Fisher RA. On the Probable Error of a Coefficient of Correlation Deduced from a Small Sample. *Metron.* 1921;1:3-32.

22. Doucet GE, Bassett DS, Yao N, Glahn DC, Frangou S. The Role of Intrinsic Brain Functional Connectivity in Vulnerability and Resilience to Bipolar Disorder. *Am J Psychiatry.* 2017:appiajp201717010095.
23. Martino M, Magioncalda P, Huang Z, et al. Contrasting variability patterns in the default mode and sensorimotor networks balance in bipolar depression and mania. *Proc Natl Acad Sci U S A.* 2016;113(17):4824-4829.
24. Nestor PG, Kubicki M, Nakamura M, et al. Neuropsychological variability, symptoms, and brain imaging in chronic schizophrenia. *Brain Imaging Behav.* 2013;7(1):68-76.
25. Phillips ML, Swartz HA. A critical appraisal of neuroimaging studies of bipolar disorder: toward a new conceptualization of underlying neural circuitry and a road map for future research. *Am J Psychiatry.* 2014;171(8):829-843.
26. Doucet GE, Rasgon N, McEwen BS, Micali N, Frangou S. Elevated Body Mass Index is Associated with Increased Integration and Reduced Cohesion of Sensory-Driven and Internally Guided Resting-State Functional Brain Networks. *Cereb Cortex.* 2017.
27. Miller KL, Alfaro-Almagro F, Bangerter NK, et al. Multimodal population brain imaging in the UK Biobank prospective epidemiological study. *Nat Neurosci.* 2016;19(11):1523-1536.
28. Moser DA, Doucet GE, Ing A, et al. An integrated brain-behavior model for working memory. *Mol Psychiatry.* in press;in press.
29. Smith SM, Nichols TE, Vidaurre D, et al. A positive-negative mode of population covariation links brain connectivity, demographics and behavior. *Nat Neurosci.* 2015;18(11):1565-1567.
30. Wechsler D. *Wechsler Abbreviated Scale of Intelligence-2nd edition.* San Antonio, TX: NCS Pearson; 2011.
31. Questionnaire IPA. Guidelines for the data processing and analysis of the "International Physical Activity Questionnaire". 2005; https://sites.google.com/site/theipaq/scoring-protocol.
32. Activities CoP. 2011; https://sites.google.com/site/compendiumofphysicalactivities/.
33. Schnurr PP, Spiro III A, Vielhauer MJ, Findler MN, Hamblen JL. Trauma in the lives of older men: Findings from the normative aging study. *Journal of Clinical Geropsychology.* 2002;8(3):175-187.
34. Ventura J, Lukoff D, Nuechterlein KH, Liberman RP, Green M, Shaner A. Appendix 1: Brief Psychiatric Rating Scale (BPRS) Expanded version (4.0) scales, anchor points and administration manual. *International Journal of methods in psychiatric research.* 1993;3:227-244.
35. Gardner DM, Murphy AL, O'Donnell H, Centorrino F, Baldessarini RJ. International consensus study of antipsychotic dosing. *Am J Psychiatry.* 2010;167(6):686-693.